REPORT DOCUMENTATION PAGE

Form Approved OMB NO. 0704-0188

1. REPORT DATE (DD-MM-YYYY)	2. REPORT TYPE	3. DATES COVERED (From - To)
14-10-2015	Ph.D. Dissertation	-

4. TITLE AND SUBTITLE	5a. CONTRACT NUMBER
MAGNETOTRANSPORT AND REMOTE SENSING OF MICROWAVE REFLECTION OF TWO DIMENSIONAL ELECTRON SYSTEMS UNDER MICROWAVE EXCITATION	W911NF-14-2-0076
	5b. GRANT NUMBER
	5c. PROGRAM ELEMENT NUMBER
	611102

6. AUTHORS	5d. PROJECT NUMBER
Tianyu Ye	
	5e. TASK NUMBER
	5f. WORK UNIT NUMBER

7. PERFORMING ORGANIZATION NAMES AND ADDRESSES	8. PERFORMING ORGANIZATION REPORT NUMBER
Georgia State University Research Foundati PO Box 3999 Atlanta, GA 30302 -3999	

9. SPONSORING/MONITORING AGENCY NAME(S) AND ADDRESS (ES)	10. SPONSOR/MONITOR'S ACRONYM(S)
	ARO
U.S. Army Research Office P.O. Box 12211 Research Triangle Park, NC 27709-2211	11. SPONSOR/MONITOR'S REPORT NUMBER(S)
	65487-EL-H.5

12. DISTRIBUTION AVAILIBILITY STATEMENT

Approved for public release; distribution is unlimited.

13. SUPPLEMENTARY NOTES

14. ABSTRACT

This dissertation summarizes three research projects related to microwave radiation induced electron transport properties in the GaAs/AlGaAs two dimensional electron systems. In chronological order, the projects are: a microwave reflection and electron magneto-transport correlation study, the combined microwave power and polarization dependence on microwave radiation induced magneto-resistance oscillations study, and a comparative study about the effect of circularly polarized and linearly polarized microwaves radiation on magneto-resistance oscillations induced due to

15. SUBJECT TERMS

GaAs/AlGaAs devices, 2D electron system, microwave, terahertz, magnetotransport, reflection, sensor, polarization , zero resistance staates

16. SECURITY CLASSIFICATION OF:			17. LIMITATION OF ABSTRACT	15. NUMBER OF PAGES	19a. NAME OF RESPONSIBLE PERSON
a. REPORT	b. ABSTRACT	c. THIS PAGE			Ramesh Mani
UU	UU	UU	UU		19b. TELEPHONE NUMBER
					404-413-6007

Report Title

MAGNETOTRANSPORT AND REMOTE SENSING OF MICROWAVE REFLECTION OF TWO DIMENSIONAL ELECTRON SYSTEMS UNDER MICROWAVE EXCITATION

ABSTRACT

This dissertation summarizes three research projects related to microwave radiation induced electron transport properties in the GaAs/AlGaAs two dimensional electron systems. In chronological order, the projects are: a microwave reflection and electron magneto-transport correlation study, the combined microwave power and polarization dependence on microwave radiation induced magneto-resistance oscillations study, and a comparative study about the effect of circularly polarized and linearly polarized microwaves radiation on magneto-resistance oscillations induced due to the microwave. These three research projects experimentally address many interesting issues in the non-equilibrium low dimensional electron transport under microwave irradiation and provide potential applications of utilizing microwave radiation induced magneto-resistance oscillations in two dimensional electron systems as a method to detect different qualities of microwaves or terahertz waves.

MAGNETOTRANSPORT AND REMOTE SENSING OF MICROWAVE REFLECTION OF
TWO DIMENSIONAL ELECTRON SYSTEMS UNDER MICROWAVE EXCITATION

by

TIANYU YE

Under the Direction of Ramesh Mani, Ph.D.

ABSTRACT

This dissertation summarizes three research projects related to microwave radiation induced electron transport properties in the GaAs/AlGaAs two dimensional electron systems. In chronological order, the projects are: a microwave reflection and electron magneto-transport correlation study, the combined microwave power and polarization dependence on microwave radiation induced magneto-resistance oscillations study, and a comparative study about the effect of circularly polarized and linearly polarized microwaves radiation on magneto-resistance oscillations induced due to the microwave. These three research projects experimentally address many interesting issues in the non-equilibrium low dimensional electron transport under microwave irradiation and provide potential applications of utilizing microwave radiation induced magneto-resistance oscillations in two dimensional electron systems as a method to detect different qualities of microwaves or terahertz waves.

INDEX WORDS: Two dimensional electron system, Magneto-transport, Microwave radiation induced zero resistance states, Microwave radiation induced magneto-resistance oscillations, Microwave reflection, Microwave power dependence, Microwave linear polarization dependence, Microwave circular polarization dependence

MAGNETOTRANSPORT AND REMOTE SENSING MICROWAVE REFLECTION OF TWO

DIMENSIONAL ELECTRON SYSTEMS UNDER MICROWAVE EXCITATION

by

TIANYU YE

A Dissertation Submitted in Partial Fulfillment of the Requirements for the Degree of

Doctor of Philosophy

in the College of Arts and Sciences

Georgia State University

2015

MAGNETOTRANSPORT AND REMOTE SENSING OF MICROWAVE REFLECTION OF

TWO DIMENSIONAL ELECTRON SYSTEMS UNDER MICROWAVE EXCITATION

by

Tianyu Ye

Committee Chair:		Ramesh Mani
Committee:		Unil Perera
		Alexander Kozhanov
		Yohannes Abate
		Douglas Gies

Electronic Version Approved:

Office of Graduate Studies
College of Arts and Sciences
Georgia State University
May 2015

DEDICATION

To the dream of becoming a physicist started from my childhood.

ACKNOWLEDGEMENTS

TABLE OF CONTENTS

LIST OF FIGURES

LIST OF ABBREVIATIONS

- 2DES - Two Dimensional Electron System

- DOS - Density of State

- GaAs/AlGaAs - Gallium Arsenide/Aluminium Gallium Arsenide

- LED - Light Emitting Diode

- LLs - Landau Levels

- MBE - Molecular Beam Epitaxy

- MOS - Metal Oxide Semiconductor

- MRIZRS - Microwave Radiation Induced Zero-Resistance State

- MRIMOs - Microwave Radiation Induced Magneto-resistance Oscillations

- MROs - Microwave Reflection Oscillations

- MW - Microwave

- QHE - Quantum Hall Effect

- SDH - Shubnikov-de Hass

- VTI - Variable Temperature Insert

- ac - Alternating current

- c.m. - Center of Mass

- dc - Direct current

- *et al.* - et alii (and others)

- etc. - et cetera (and the rest)

- i.e. - id est (that is)

- ref. - reference

- w/ - With

- w/o - Without

Chapter 1

INTRODUCTION

1.1 Structure of this dissertation

This dissertation contains five chapters. The first chapter introduces the structure of this dissertation, as well as the background of my Ph.D. research projects. The background section contains three different sections. Under the first section, I will present basic ideas of two dimensional electron system (2DES), which is realized in the GaAs/AlGaAs heterostructure samples used in these projects. As well, I will introduce the basic electron transport measurement setup under this section. Under the second section, I will introduce a broadened background about the physics phenomenon, namely, the Quantum Hall Effect, in 2DES. Under the third section, I will introduce the specific research area of this dissertation, microwave radiation induced magneto-transport properties in the 2DES. Under this section, I will briefly introduce the experimental and theoretical aspects of this area and briefly assert the motivation of the research work included in this dissertation.

The second chapter through the fourth chapter follows a chronological order to describe three different but related research projects of my Ph.D. research.

The second chapter summarizes the magneto-transport study and concurrent microwave reflection in the 2DES utilizing two different methods. One method employs a carbon resistor as a remote sensor and the other method employs a microwave power meter to measure the microwave reflection from the 2DES. Results from these two methods will be exhibited in two parts and will be discussed respectively. Correlation between the microwave reflection and electron transport property has been examined.

The third chapter exhibits a combined study of microwave power and polarization dependence of microwave radiation induced magneto-resistance oscillation (MRIMOs). Here, electron transport properties have been examined as a function of both microwave power and linearly polarized microwave polarization angle.

The fourth chapter describes a study of the effect of circularly polarized microwaves and linearly polarized microwaves on the MRIMOs in 2DES. Electron transport under different types of microwave radiation has been examined comparatively.

Finally, the fifth chapter summarizes the major conclusions drawn from these projects and briefly describes the significance of these works and their contributions.

1.2   Material basics and measurement basics

1.2.1   2DES basics
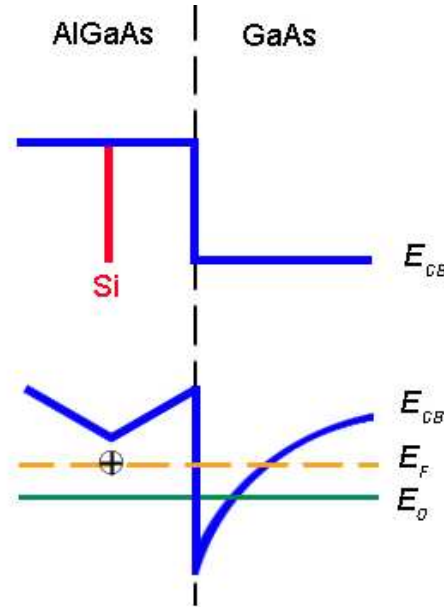
Figure 1.1. Schematic description of modulation doped GaAs/AlGaAs heterostructure including a 2DES. The top panel indicates the large difference between AlGaAs and GaAs conduction band E_{CB}. Si atoms are doped in AlGaAs at a distance away from the interface. Electrons from Si donor are transferred to GaAs side. The lower panel shows the equilibrium state after the charge transfer. In the figure, the blue solid lines are the conduction band, the green solid line is the ground state of electrons and the yellow dashed line is the Fermi Level.

When electrons are placed into a "flatland" they form a 2DES. Many milestones in condensed matter physics were discovered using the 2DES, milestones such as the Integer Quantum Hall Effect [1], the Fractional Quantum Hall Effect [2,3], the Radiation Induced Zero-resistance states [4] and Graphene [5]. Traditionally, 2DES are realized in silicon MOS and GaAs/AlGaAs heterostruc-

ture or GaAs/AlGaAs quantum well. The 2DES used in my Ph.D. research is buried within a GaAs/AlGaAs heterostructure. Layered heterostructures used in these experiments are commonly fabricated by molecular beam epitaxy (MBE) [6] in a very clean environment. For such a heterostructure, the larger bandgap of AlGaAs leads to its conduction band energy being higher than GaAs. A modulation-doped method, which means dope Si atoms in the AlGaAs at a distance away from the interface, is adopted to transfer the electron from the donor to the lower energy conduction band of GaAs, see Fig. 1.1. Therefore, 2DES is separated from the doped AlGaAs region by an undoped AlGaAs layer to minimize electron scattering by the ionized impurities. The quality of 2DES is characterized by its mobility μ. Typically the low-temperature mobility of GaAs/AlGaAs heterostructure 2DES is more than $10^6 cm^2$/Vs. To reach that high mobility, the material needs to eliminate interface irregularities, ionized impurities etc., which rely on the vacuum integrity of the MBE growth chamber and the cleanliness and purity of the source materials and the GaAs substrate.

1.2.2 Measurement basics

The 2DES reaches a high mobility state only at low temperature, which can be realized by a cryostat. Fig. 1.2 exhibits a brief schematic diagram of a typical cryostat. It consists of a big stainless steel tank with a vacuum insulating shield on the outside. The tank is filled with liquid helium, which is at a temperature of 4.2 K. As the tank is covered on the top and pumped on the helium surface, the temperature inside the liquid helium could drop down to as low as 1.5 K. A coiled superconducting magnet lies at the bottom of the cryostat and is immersed in liquid helium. A variable magnetic field in the perpendicular direction can be supplied by this magnet. 2DES samples are mounted at the end of a long sample holder, which can bring the sample in to the center bore of the coil magnet inside the cryostat. Specifically, for my measurements, a cylindrical microwave waveguide is also mounted at the center of the sample holder to send microwave from the top of sample holder to the sample, since microwaves are involved in all of my measurements.

Typical electron transport measurements are carried out by low noise measurements, also known as low frequency lock-in techniques, see Fig. 1.3. 2DES samples with metal contacts are wired up with lock-in amplifiers. A low-frequency ac current, I_{ac}, is passed through the sample from source contact to drain contact. The lock-in amplifier is used as a voltage meter to measure
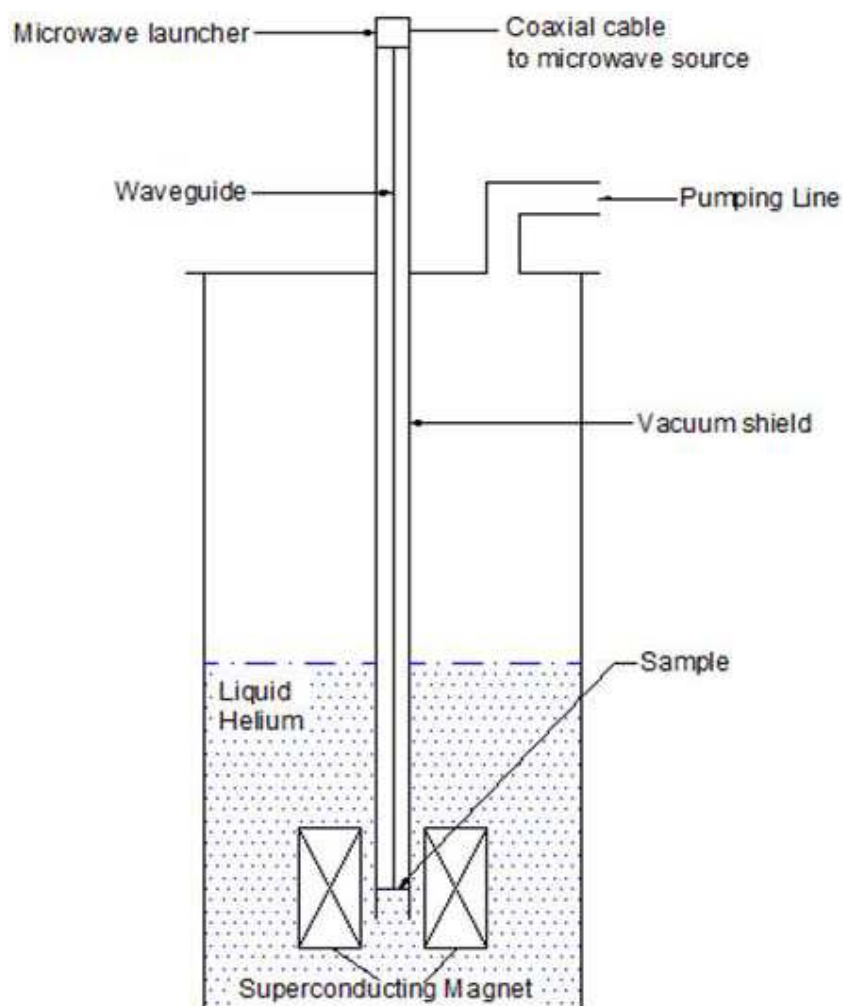
Figure 1.2. Schematic diagram of liquid helium cryostat. When the liquid helium is pumped, sample temperature could be as low as 1.5 K. The attached microwave components are special for microwave related measurements, which will be described in Chapters 2 through 4, but are not necessary in low temperature magneto-transport measurements.
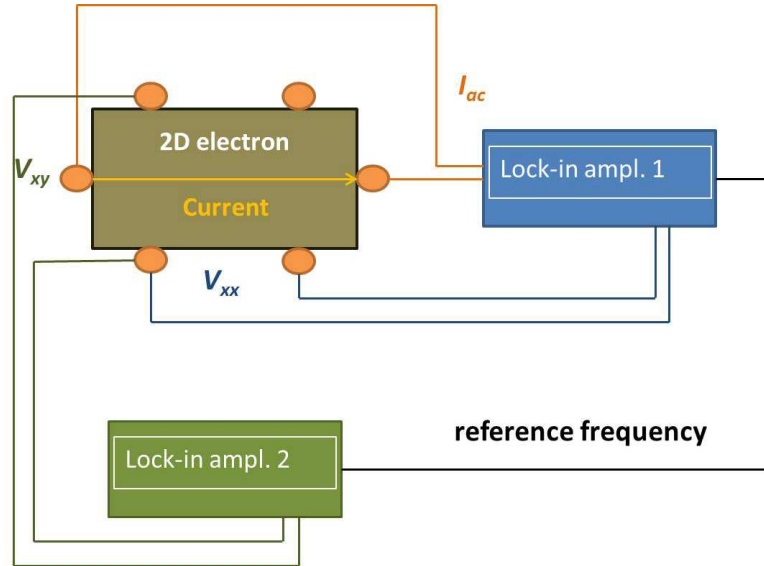
Figure 1.3. Schematic diagram of the lock-in technique to measure electric properties. The dark yellow rectangular shape is the top view of 2DES hall bar sample. The six orange color circles are gold/germanium alloy contacts. Low frequency current I_{ac} is sent from source contact to drain contact. Lock-in amplifier 1 measures the longitudinal voltage, V_{xx}, and lock-in amplifier 2 measures the transverse voltage/Hall voltage, V_{xy}. Dividing both voltages by I_{ac} gives the longitudinal resistance, R_{xx} and Hall resistance, R_{xy}. Lock-in amplifier 1 uses the internal frequency as a reference signal to lock the ac signal but lock-in amplifier 2 needs an external reference signal from lock-in amplifier 1 to lock the ac signal.

longitudinal voltage drop as V_{xx}. In the same way, transverse voltage drop could be measured by another lock-in amplifier as V_{xy}. Here, the function of lock-in amplifier is to detect the voltage signal in the frequency of I_{ac} but filter out other frequencies. Because, commonly, the applied current I_{ac} is in the range of μA, therefore, the measured V_{xx} and V_{xy} values are also small, commonly in μV. Lock-in amplifiers provide a high signal to noise ratio.

1.3   Quantum Hall Effect
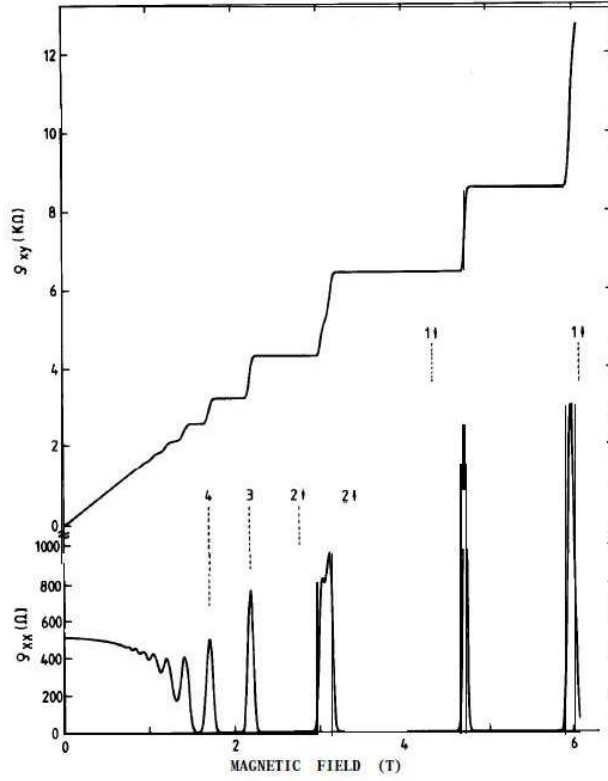
Figure 1.4. Hall resistivity, ρ_{xy} (top panel) and Longitudinal resistivity, ρ_{xx} (bottom panel) as functions of magnetic field B. ρ_{xy} exhibit plateaus when ρ_{xx} meets zero resistance or minima of SDH oscillations. (After von Klitzing [7])

When a conductor is subject to a perpendicular magnetic field, as the magnetic field increases, the Hall voltage/transverse voltage also will linearly increase, because of the increasing of Lorentz force on electrons. Comparatively, at very low temperatures, if a 2DES is subject to a perpendicular magnetic field, its Hall resistivity will still increase as the magnetic field increases, but it exhibits plateaus at certain magnetic field levels. Whenever Hall resistivity exhibit plateaus, the oscillatory

longitudinal resistivity trace exhibits zero or minimum values, see Fig. 1.4. The oscillations in longitudinal signal are called Shubnikov-de Hass (SDH) oscillations and they are periodic in $1/B$, where B is the magnetic field. Commonly, in order to observe QHE and SDH oscillations, measurement condition has to meet

$$\hbar\omega_c \gg k_B T \qquad (1.1)$$

where $\hbar$ is the Planck constant, ω_c is the cyclotron resonance frequency, k_B is the Boltzmann constant, and T is temperature. Thus, very low temperature is necessary to observe QHE and SDH oscillations. Moreover, the Hall conductivity value of the plateaus are at the integer times or certain fractional times e^2/h, i.e.,

$$\sigma_{xy} = \nu e^2/h \qquad (1.2)$$

where σ_{xy} is the Hall conductivity, ν is the filling factor that indicate how many LLs has been filled up, e is the electron charge, and h is the Planck constant [1].
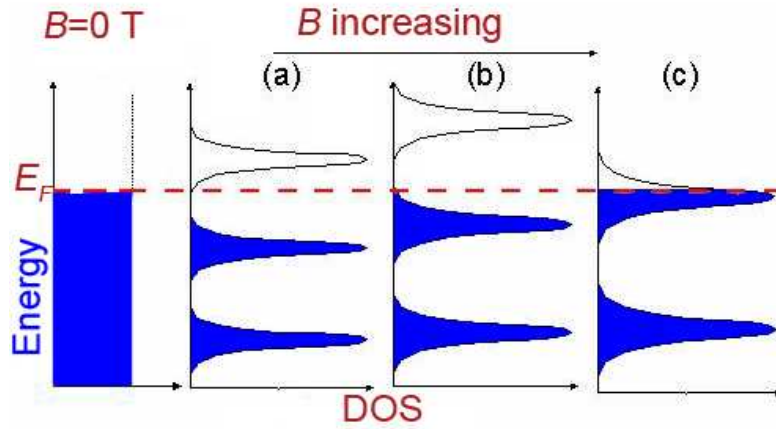
Figure 1.5. 2DES energy as a function of density of states. Red dashed lines indicate the Fermi Level. At zero magnetic field, the energy spectrum of 2DES is continuous and the DOS are the same for electrons with different energy. Once the magnetic field starts to increase, the electron energy starts to split into Landau Levels. As the magnetic field further increases, each Landau Level occupies more DOS. In panel (a) and (b) the Fermi Level occurs at the minima of DOS, which means electrons are filling up right to localized states and there is no current carried by electrons. In panel (c) the Fermi Level occurs at almost the maximum of DOS, which means that electrons are filling up to the extended state and then current is carried by the majority electrons. (After ref. [8])

In a perpendicular magnetic field, electrons in 2DES make orbital motion with a certain allowed quantized energies, which are called Landau Levels (LLs). The LLs are quantized by

$$(N + 1/2)\hbar\omega_c \tag{1.3}$$

where N is an integer and

$$\omega_c = eB/m^* \tag{1.4}$$

is the cyclotron frequency and $m^* \approx 0.067m_0$ is the effective mass of 2D electrons in GaAs. In the absence of a magnetic field, the electron DOS is a continuous function of electron energy, see the left panel of Fig. 1.5. Electrons distribute evenly over every energy level up to Fermi Level, which is the highest energy level electrons could occupy. Once the perpendicular magnetic field is applied to 2DES, the continuous electron energy spectrum changes to split levels, which are LLs. Ideally, LLs are delta functions. However, in the presence of impurities, the LLs are broadened, see Fig. 1.5 (a)-(c). The states in the tails of LLs are localized states and the ones in the center of LLs are extended states, which carry current through the 2DES. Each LL occupies electron

$$DOS = eB/h \tag{1.5}$$

As magnetic field, B, increases, each LL occupies more DOS. Since the Fermi level stays the same, it seems like there are fewer LLs below Fermi level. When this change in the filling effect is happening, the Fermi level periodically experiences the localized state and extended state of LLs, which makes the magneto-resistivity/conductivity periodically change. At low magnetic field, adjacent LLs are not well resolved and each LL occupies a small DOS. Therefore, the SDH oscillation amplitudes are very small and will not reach zero resistance states.

1.4 Microwave radiation induced magneto-transport properties in 2DES

1.4.1 MRIZRS and MRIMOs

Based on the measurements mentioned above, see Fig. 1.2, if additional microwave illumination is applied onto the surface of 2DES, the 2DES can reach zero-resistance states even at low magnetic
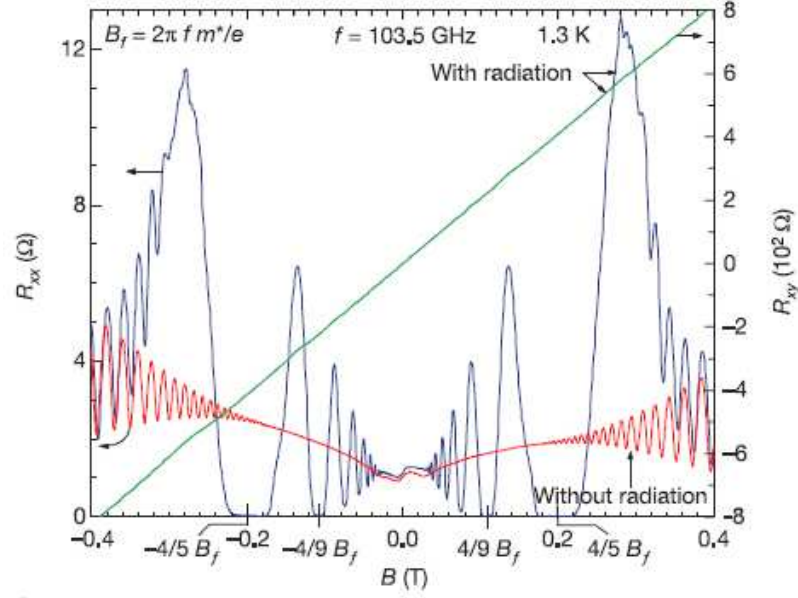
Figure 1.6. Longitudinal resistance R_{xx} (plot on the left scale) and Hall resistance R_{xy} (plot on the right scale) as functions of magnetic field. Blue and green curves are under 103.5 GHz microwave radiation. The red curve is without microwave radiation. The red R_{xx} only exhibits SDH oscillations and blue R_{xx} curve exhibits MRIMOs and MRIZRS. The green R_{xy} curve does not exhibit any obvious plateaus. (After Mani *et al.* [4])
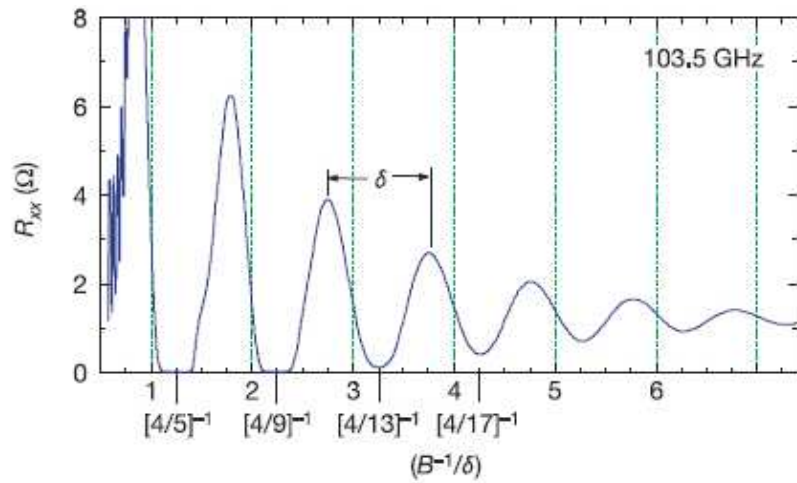
Figure 1.7. Longitudinal resistance R_{xx} as a function of normalized B^{-1}. Here δ is the oscillatory period in B^{-1} and zero resistance states or resistance minima are at $[4/(4j+1)]^{-1}$ with $j = 1, 2, 3....$ (After Mani *et al.* [4])

fields and its magneto-resistance can exhibits a huge oscillatory modulation on SDH oscillations, see Fig. 1.6. These are known as microwave radiation induced zero-resistance states (MRIZRS) [4] and microwave radiation induced magneto-resistance oscillations (MRIMOs) [4, 9]. MRIMOs are periodic in $1/B$ and the oscillations yield a 1/4-cycle shift [10], see Fig. 1.7, where the zero resistance states or oscillation minima occur at

$$B = [4/(4j+1)]B_f \tag{1.6}$$

(j is an integer), where

$$B_f = 2\pi f m^*/e \tag{1.7}$$

f is microwave frequency, m^* is effective mass of the electrons in GaAs, and e is electron charge. Or in another expression,

$$\frac{1}{B} = (j + \frac{1}{4})\frac{e}{2\pi f m^*} \tag{1.8}$$

The MRIMOs and SHD oscillations both appear at low magnetic fields and both exhibit periodicity in $1/B$. However, there is an obvious difference between QHE and MRIMOs: when the R_{xx} exhibits a zero resistance state or minimum of oscillations, R_{xy} does not exhibit any plateaus. This feature indicates the physical scheme of MRIMOs and MRIZRS may not be limited by the filling effect of using Fermi Level to fill up LLs, because the localized states are not well resolved at low magnetic field.

1.4.2 Theoretical approaches

MRIZRS and MRIMOs have been studied experimentally [11–43] and theoretically [44–70] from different aspects. Up to now there are mainly three different understandings about MRIZRS and MRIMOs: the displacement model [44–46], the inelastic model [51], and the radiation driven electron orbital model [50].

The displacement model [44–46] describes radiation-assisted indirect inter-Landau-level scattering by phonons and impurities. In Lei *et al.*'s formulation of the displacement model [46] they consider that the center-of-mass (c.m.) of the whole 2DES in a magnetic field performs a cyclotron motion modulated by the high frequency field of frequency ω. There exists coupling between this
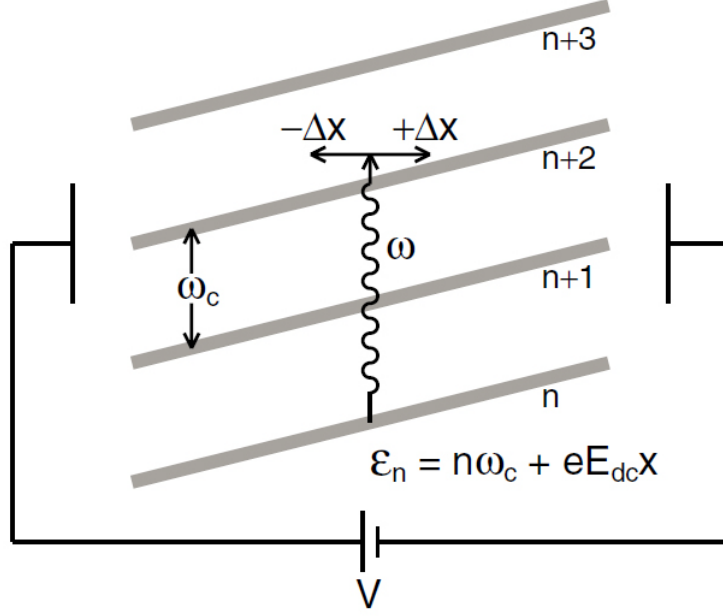
Figure 1.8. Schematic diagram of the displacement model. LLs are tilted by a dc bias across 2DES sample. Photon energy ω excites electron from lower LL to higher LL and electrons are scattered by disorders to the left or right by a distance $\pm\Delta x$. If the final DOS to the left exceeds that to the right, dc current is enhanced and conductivity will be increased. And vice versa. (After Durst *et al.* [44])

c.m. motion and the relative motion of the two dimensional electrons due to the impurities or phonon scatterings. The high frequency field affects, through the coupling, the relative motion of electrons by creating additional channels for electron transition between different states (LLs). The calculated result of displacement model [44] gives a relation

$$\Delta\sigma_{xx} \propto -sin(2\pi\omega/\omega_c) \tag{1.9}$$

which indicates an oscillatory conductivity. As shown in Fig. 1.8, LLs are tilted when 2DES is subject to a voltage bias across its source and drain contacts. The separation between each LL is the cyclotron resonance frequency, ω_c. Once an electron is excited by microwaves with frequency ω, the electron will be excited from a lower LL to a higher LL. When this excitation happens between integer times of LLs, there is no change in the resistivity of 2DES. However, when the excitation ends up in between LLs, the impurities in 2DES will spatially scatter electrons forward

or backward to the adjacent LLs, which will assist or resist electron transport, thus producing oscillatory magneto-resistance.
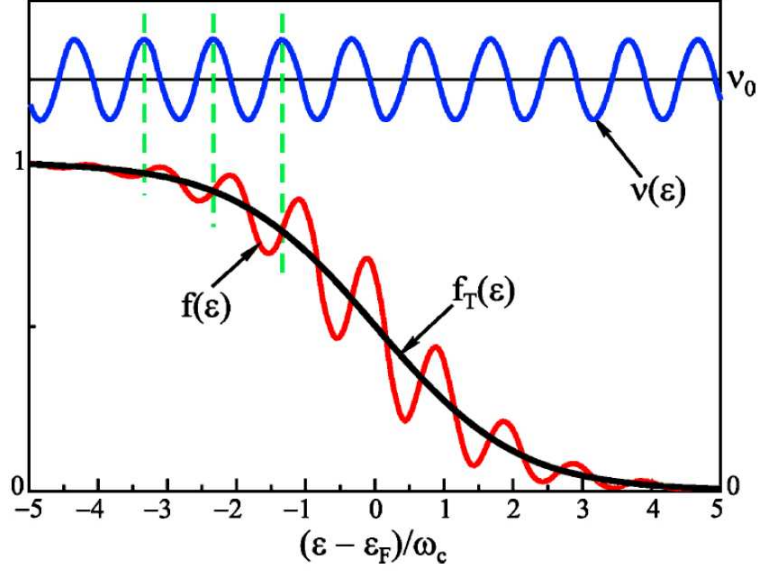
Figure 1.9. Schematic diagram of the inelastic model. Oscillatory DOS $\nu(\varepsilon)$ (blue curve) and radiation induced distribution function oscillation $f(\varepsilon)$ as a function of electron energy normalized by cyclotron resonance energy ω_c.(After Demitriv *et al.* [51])

The inelastic model [51] proposed an effect of a radiation-induced steady state non-equilibrium distribution in 2DES, see Fig. 1.9. The inelastic model [51] starts from Druid conductivity σ_ω^D and considers a stationary kinetic equation

$$St_\omega(f) + St_{dc}(f) = -St_{in}(f) \tag{1.10}$$

where St_ω represents the effect of microwaves, St_{dc} represents the dc field, and St_{in} represents inelastic relaxation. By solving the non-equilibrium distribution function $f(\varepsilon)$ as a solution to the kinetic function and including the inelastic processes in the Fermi distribution $f_T(\varepsilon)$ they found out the final expression of the photo-conductivity in the format of

$$\frac{\sigma_{ph}}{\sigma_{dc}^D} = 1 + 2\delta^2 \left[1 - \frac{P_\omega \frac{2\pi\omega}{\omega_c} \sin\frac{2\pi\omega}{\omega_c} + 4Q_{dc}}{1 + P_\omega \sin^2\frac{\pi\omega}{\omega_c} + Q_{dc}} \right] \tag{1.11}$$

where P_ω and Q_{dc} are convenient dimensionless notations for the strength of the ac and dc fields and factor

$$\delta = \exp\left(\frac{\pi}{\omega_c \tau_q}\right) \tag{1.12}$$

and τ_q is the zero B-field single-particle relaxation time. This gives the photo-conductivity σ_{ph} and oscillatory part. In Fig. 1.9, the solid black curve shows the distribution function of 2DES without microwaves and it exhibits a smooth Fermi Distribution $f(\varepsilon)$. Under the effect of both dc (current through sample) and ac (microwave illumination) electric fields, the modulation f_{osc} is added onto the distribution function and it is periodic in $1/\omega_c$. This leads to the photo-conductivity oscillations.
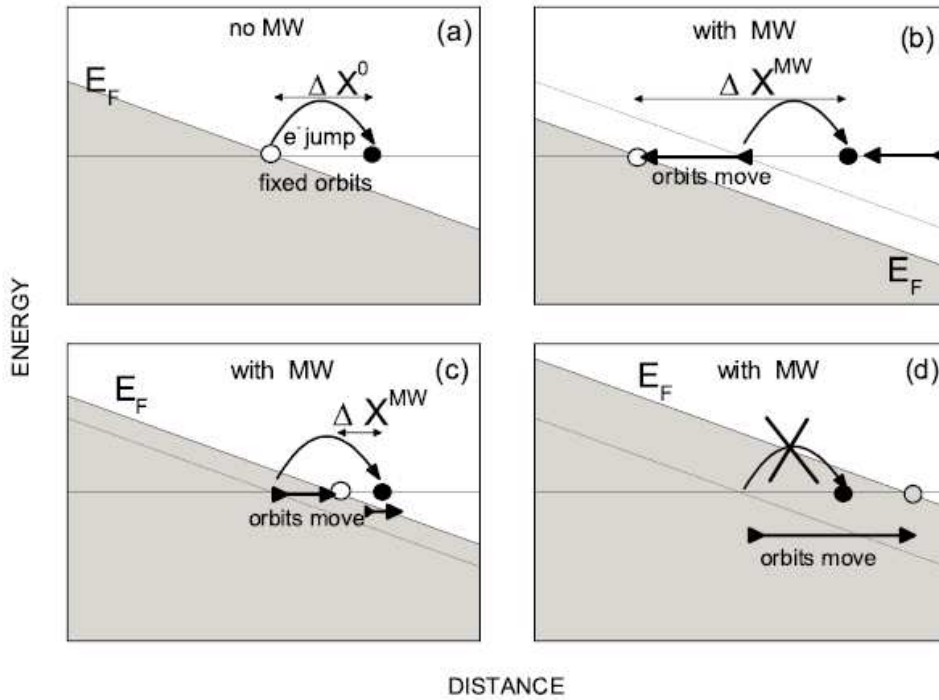
Figure 1.10. Schematic diagram of the radiation driven electron orbital model. (a) is the electron jump case without microwave radiation. (b)-(d) are electron jump cases with microwave radiation. (b) is the case of electron jump being lengthened and (c) is the case of electron jump being shortened. (d) is the electron jump forbidden case. (After Inarrea et al. [50])

The radiation driven electron orbital model [50] considers the periodic motion of the electron orbit centers under irradiation, see Fig. 1.10. In this model, Inarrea et. al. developed a semi-classical model based on the exact solution of the electronic wave function in the presence of a static field B interacting with microwave radiation. In this model, they also considered a quantum forced

harmonic oscillator and a perturbation treatment for elastic scattering from randomly distributed charged impurities. They formalized their Hamiltonian as

$$H = H_1 - eE_0 \cos \omega t X \tag{1.13}$$

where X is the center of orbit for the electron spiral motion and H_1 is the Hamiltonian corresponding to a forced harmonic oscillator, whose orbit is centered at X. The classical solution of the forced harmonic oscillator is

$$x_{cl}(t) = \frac{eE_0}{m^* \sqrt{(\omega_c^2 - \omega^2)^2 + \gamma^4}} \cos \omega t \tag{1.14}$$

where E_0 is the radiation electric field and γ is a damping factor for the electronic interaction with acoustic phonon. The average effective distance advanced by electron in every scattering jump is

$$\Delta X^{MW} \propto x_{cl} \tag{1.15}$$

and the final longitudinal conductivity σ_{xx} is given by

$$\sigma_{xx} \propto \int dE \frac{\Delta X^{MW}}{\tau} \tag{1.16}$$

where E is energy and τ is scattering time. After some algebra, they found

$$R_{xx} \propto \frac{eE_0}{m^* \sqrt{(\omega_c^2 - \omega^2)^2 + \gamma^4}} \cos \omega t \tag{1.17}$$

In absence of microwaves, electrons in 2DES jump between fixed orbits due to scattering. But when microwaves are applied onto the 2DES, electron orbits are driven by microwaves to move either backward or forward. The oscillation of electron orbits could make the electron jump for a longer distance or shorter distance, which appears like smaller or bigger resistance, respectively. When the forward moving electron orbits move beyond the electron jump, the electron jump is forbidden. Thus, zero resistance states show up.
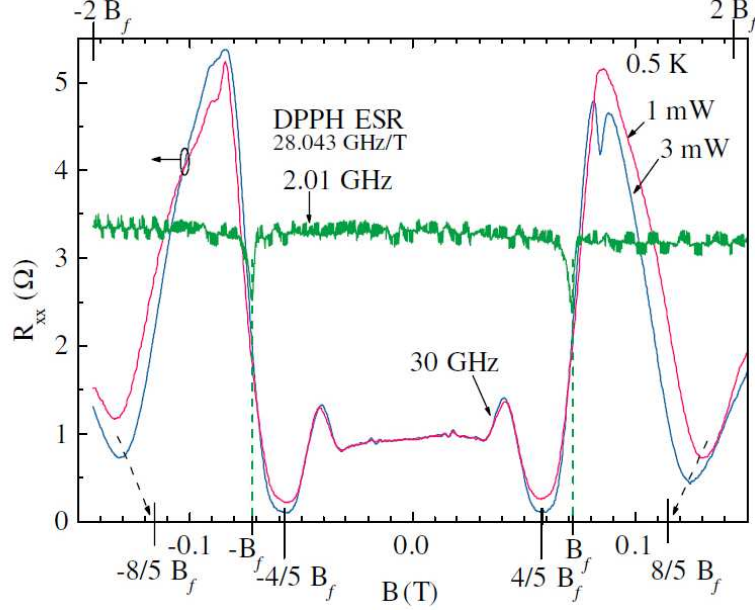
Figure 1.11. The magneto-resistance R_{xx} is plotted vs the magnetic field B for a GaAs/AlGaAs device under photo-excitation at f=30 GHz. Also shown is the electron spin resonance of diphenyl-picryl-hydrazal at 2.01 GHz, which marks $B_f = 2\pi f m^*/e$. R_{xx} exhibits neither a maximum nor a minimum at B_f. (After Mani *et. al.* [10])

1.5 Research status and motivation

After MRIMOs were discovered, the first clarification of this phenomenon is the phase shift of the zero resistance state [10], and it was clearly found to be a 1/4-cycle shift [10] on the period of MRIMOs, see Fig. 1.11. As well, different dependences of MRIMOs were explored. The temperature dependence [4] indicates that the amplitude of MRIMOs increases as temperature drops. Microwave power dependence studies found that the amplitude of MRIMOs increases as microwave power increases, see Fig. 1.12. Note that the inelastic model predicts that the relation between MRIMOs amplitude and microwave power should be linear; however, the radiation driven electron orbital model [56] indicated it should be non-linear. Some experiments [30] have explored this issue. By fitting MRIMOs with a fitting function

$$\Delta R_{xx} = -A \exp(-\lambda/B) \sin(2\pi F/B) \tag{1.18}$$

and extracting the amplitude A, the MRIMOs amplitudes are found to increase non-linearly with the microwave power. Here, λ is the damping parameter, and F is the f-dependent magneto-resistance oscillation frequency. Microwave frequency dependence studies indicate MRIMOs shift to higher magnetic fields as the microwave frequency increases. Drive current dependence [4] studies found MRIMOs amplitude stay unchanged as the drive current changes. Recent microwave polarization dependent study [32, 34] reveals that MRIMOs depend on the polarization direction of linearly polarized microwaves, see Fig. 1.13. This observation has also been confirmed theoretically by the displacement model [64] and the radiation driven electron orbital model [68].
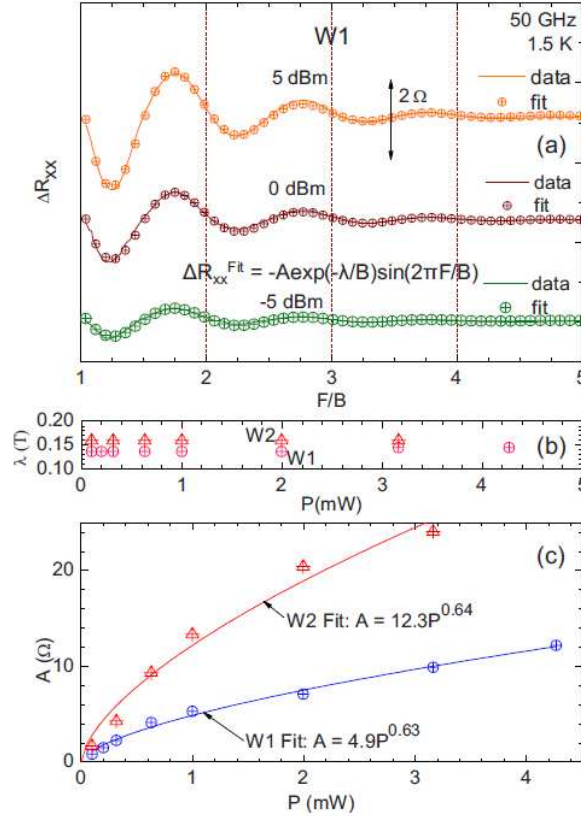
Figure 1.12. (a) Relative longitudinal resistance ΔR_{xx} plotted as a function of F/B (F is microwave frequency and B is magnetic field) at different microwave powers. Circles represent the data and solid lines are the fittings using $\Delta R_{xx} = -A\exp(-\lambda/B)\sin(2\pi F/B)$ (b) λ is plotted vs P. (c) The lineshape amplitude, A, is plotted vs P. Also shown are fits, $A = A_0 P^\alpha$.(After Mani $et.$ $al.$ [30])

Moreover, there are other open questions in the MRIMOs. One of them relates to the microwave absorption and reflection. Both the displacement model [49] and radiation driven electron orbital model [57] predict a periodic change of microwave absorption as B sweeps, but such a change has

never been experimentally observed. Another one is the role of microwave power in MRIMOs. Because there are contradictory predictions made by different theoretical models, a systematic study of microwave power dependence is also necessary to clarify the problem. Furthermore, in a recent study [34] of polarization dependence, there are some unusual results, which indicate that the microwave power dependence may not be just a simple linear or non-linear relation. A third issue is the polarization dependence, because prior to this work, most of the research interest focused on the linearly polarized microwave radiation. MRIMOs reaction under circularly polarized microwaves is still a mystery.
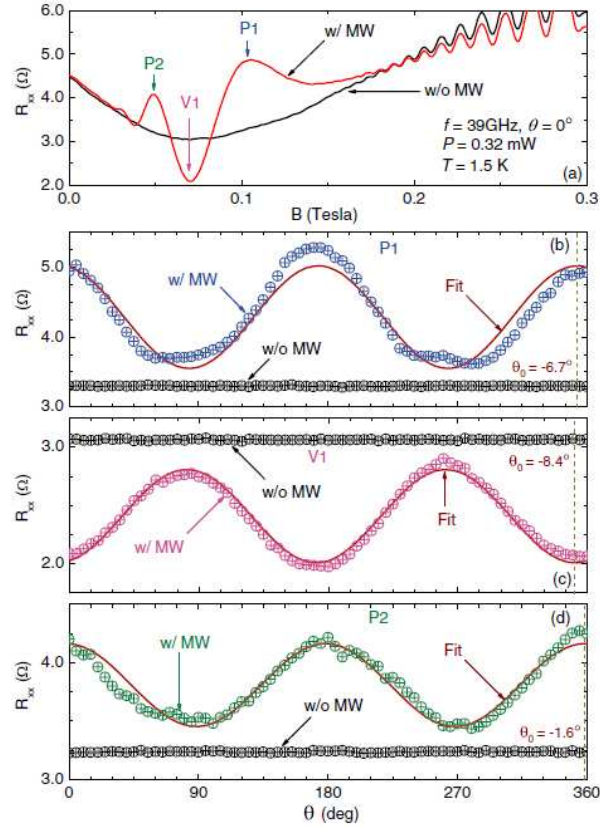
Figure 1.13. Dark and microwave excited magneto-resistance R_{xx} are exhibited here. The experimental extremal R_{xx} response at field strength of (b) P1, (c) V1, and (d) P2. (b) and (d) show that, at the maxima P1 and P2, R_{xx} under photo-excitation exceeds the dark R_{xx}. On the other hand, at V1, the R_{xx} under photo-excitation lies below the dark R_{xx}.(After Ramanayaka et al. [34])

In summary, my research project focused on the experimental observation of microwave reflection from 2DES, microwave power dependence and polarization dependence. Such studies yield many results that are applicable beyond their scientific interest. For example, most of the contem-

porary microwave detectors can only detect a narrow band width power range. With the help of MRIMOs in 2DES, one might be able to characterize different properties of detected microwaves, such as microwave power, frequency and polarization etc.. Therefore, a thorough study of MRIMOs is necessary for the further application of 2DES.

Chapter 2

REMOTE SENSING OF MICROWAVE REFLECTION FROM 2DES

2.1 Introduction

The MRIMOs effect has been studied for several years. In the past, people have studied various aspects of MRIMOs, such as its temperature dependence [4], microwave power dependence [30], microwave frequency dependence [4] and microwave polarization dependence [32, 34]. All these studies enriched details of the physical contributions to the MRIMOs, and on the other hand, provided physical background toward its application. Since the MRIMOs are dealing with microwave or terahertz [36] radiation, their applications in microwave or terahertz detection are expected. Through the above discussed studies,and others [11–18, 20–38], the microwave effect on 2DES has been well studied and most of the physical properties were measured directly on the sample. Interestingly, there were preliminary experimental studies of the indirect measurements of MRIMOs carried out by Mani *et al.* [15, 16]. They exhibited the microwave reflection from 2DES and microwave transmission through 2DES. Both the reflection and the transmission are active in the regime of MRIMOs. More than that, there are different theories about MRIMOs that predict the existence of microwave absorption from 2DES. In the displacement model [49], Lei *et al.* found a correlation between microwave absorption and MRIMOs. They claimed that there is maximum microwave absorption at cyclotron resonance or its higher orders. Radiation driven electron orbit model [57] suggests that there is a huge and broadened absorption peak at the cyclotron resonance. Hereby, we carried out a systematic study of the microwave reflection from 2DES, trying to correlate the observed reflection signals with MRIMOs.

2.2 Reflection measurements by carbon sensor

2.2.1 Sample preparation and measurement details

The material we measured was GaAs/AlGaAs heterostructure including a 2DES. The material was first fabricated into a Hall bar by photo-lithography and followed by wet etching. On the edge

of the Hall bar, gold-germanium contact pads were fabricated by photo-lithography and electron beam evaporation. The fabricated sample was then mounted at the end of a sample holder. The main part of the sample holder is a long cylindrical waveguide, which is used to send microwaves onto the sample, with the device normal is oriented along the waveguide axis. For the microwave reflection measurement, a carbon resistor was placed at the end of waveguide and immediately above the sample, see Fig. 2.1 (a). It was designed to sense remotely the microwave reflection from the sample. The sample holder was then inserted into a variable temperature insert (VTI) inside the bore of a super conducting solenoid. The sample was cooled down to 1.5 K by pumping on the liquid helium surface within the VTI. In order to get a high mobility 2DES in the sample, a red light emitting diode (LED) was employed to briefly illuminate the sample. After illumination, the sample mobility reached and maintained a level as high as 8×10^6 cm^2/Vs. The electron density was 2.3×10^{11} cm^{-2}. The measurement of the high mobility sample involved a low frequency, four terminal, lock-in technique. The magneto-resistance of both sample resistances, which include the diagonal resistance and Hall resistance, and carbon resistor resistance are measured concurrently.

2.2.2 Microwave reflection test of carbon sensor

The reason why a carbon resistor was employed as a sensor here is that the carbon resistor we used exhibits a strong negative temperature coefficient, i.e.,

$$dR_s/dT < 0. \tag{2.1}$$

The carbon resistor is sensitive especially at low temperatures, (see Fig. 2.1 (b)) where a small change in temperature results in a dramatic change in sensor resistance. Therefore, heating of the carbon sensor by microwaves reflected from 2DES produces a reduction in the resistance, which becomes the signature of microwave reflection. But before one could use the sensor resistance to examine the microwave reflection, a set of experiment needs to be done in order to setup the correlation between the sensor resistance and the microwave reflection from 2DES, because the sensor was placed between the end of microwave waveguide and sample so that the sensor might sense signal from both incident microwaves or reflected microwaves.
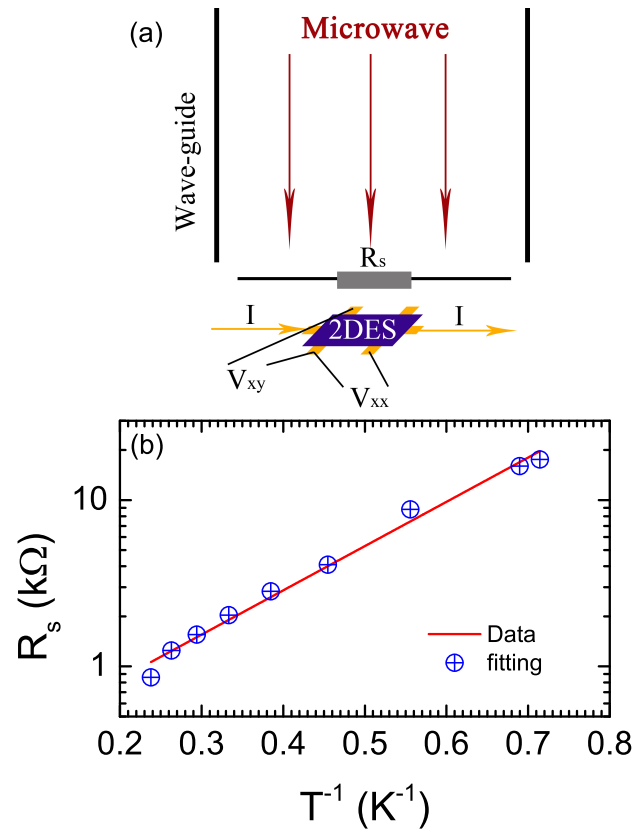
Figure 2.1. (a) A schematic of the measurement configuration showing the GaAs/AlGaAs Hall bar and the remote sensing resistor, R_s, located at the bottom of a cylindrical waveguide, within a low temperature cryostat. (b) The response curve of the carbon sensor, R_s. The red line shows that the sensors resistance increases rapidly with a reduction of temperature.
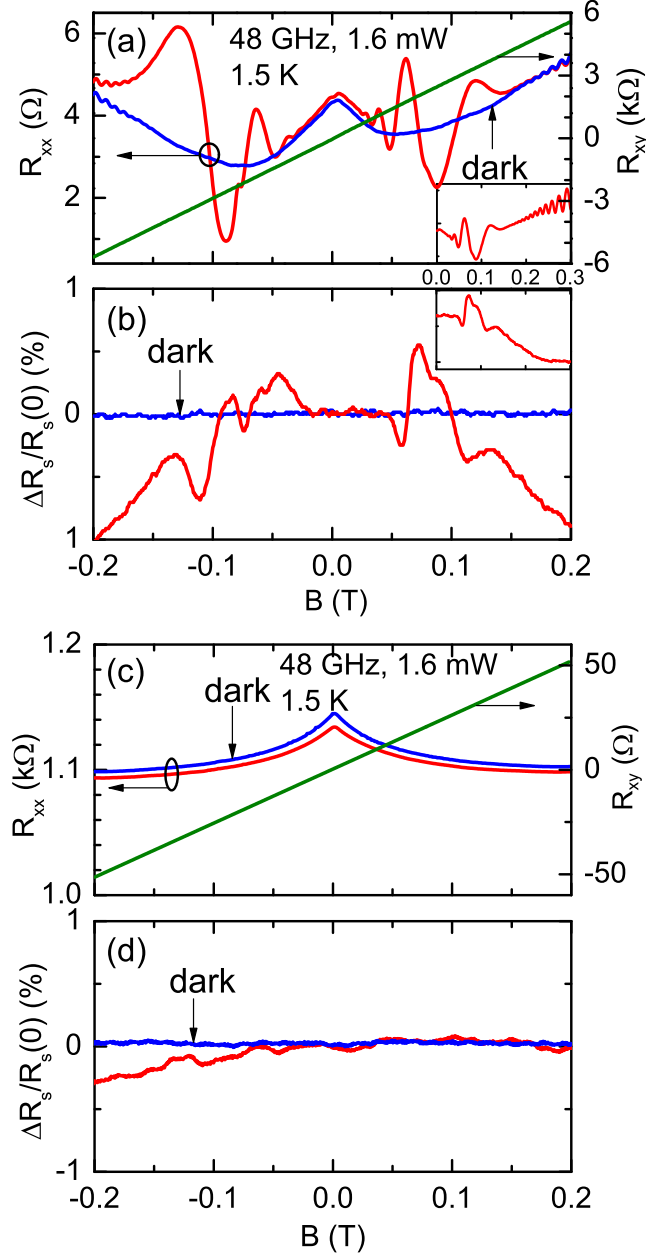
Figure 2.2. Panels (a) and (b) show the diagonal resistance (R_{xx}), Hall resistance (R_{xy}) and the fractional change of the remote detector resistance ($\Delta R_s/R_s(0)$) as functions of magnetic field, B, of sample S1. (a) R_{xx} (left scale) and R_{xy} (right scale) of S1 with (red curve) and without (blue curve) 48 GHz microwave illumination. (b) Concurrent measurement of $\Delta R_s/R_s(0)$ with (red curve) and without (blue curve) 48 GHz microwave excitation. The insets of (a) and (b) show the photo-excited R_{xx} and $\Delta R_s/R_s(0)$ signals over a broader B-range. Panels (c) and (d) show the exact same measurement under the same conditions but on a low mobility sample S2.

Fig. 2.2 (a) and (b) show the longitudinal resistance R_{xx} and sensor resistance R_s of the high mobility sample mentioned above. It is clear from the comparison between (a) and (b) that, without microwave radiation, neither R_{xx} nor R_s reveal oscillations. However, with microwave radiation (here 48 GHz was used), both R_{xx} and R_s exhibit strong oscillations between -0.2 and +0.2 T. Out of this magnetic field region, R_{xx} exhibits SDH oscillations, and R_s monotonically decreases, see insert of Fig. 2.2 (a) and (b). Note that a non-vanishing $\Delta R_s / R_s$ signal occurs not just in the vicinity of cyclotron resonance, B=0.11 T, but over nearly the entire B-span of the MRIMOs. Here the microwave induced changes in the sensor signal reach $\Delta R_s / R_s = 1\%$, where

$$\Delta R_s = R_s(B) - R_s(0) \tag{2.2}$$

From this preliminary comparison, it is clear that the structure in R_s is related to the effect of microwaves on the 2DES. However, it is difficult to tell if the oscillations in R_s are induced by the incident microwave or the reflected microwave. Therefore, similar measurements were carried out on a low mobility sample which would not reveal MRIMOs. As Fig. 2.2 (c) and (d) shows R_{xx} does not reveal any oscillation even with the same microwave radiation, and it only shifts down about 0.3 kOhm from the R_{xx} trace without microwave radiation. This shift is due to the heating effect of microwave radiation. Similarly, the R_s trace does not reveal any oscillation even with microwaves this time. This confirms that the previous microwave induced oscillation in the carbon sensor signal is not from the incident microwaves but from electron transport of the 2DES sample, which could only be microwave reflection.

2.2.3   Carbon sensor results

Fig. 2.3 shows the microwave power-dependence of the magneto-resistance of sample and sensor. The exhibited traces indicate the following features with changing microwave power: the phase of MRIMOs in R_{xx} does not change with the microwave power, but the amplitude of oscillations increases with power increase over the range $0 \leq P \leq 3.2$ mW. The oscillations in the reflection signal, which is conveyed by R_s / R_s(-0.2 T), are also in phase for different microwave powers, although the relative amplitude increases with P increases. Beside the major oscillations on the R_{xx} trace, there are also two small peaks, which are pointed out by the blue arrow in Fig. 2.3 (a), on the shoulder
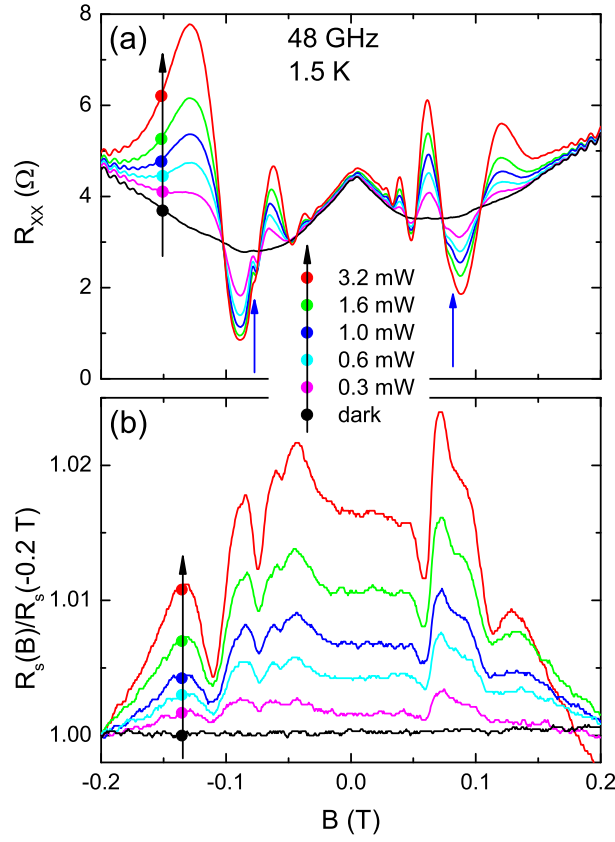
Figure 2.3. (a) The dark- and photo-excited- R_{xx} signal at 48 GHz, and (b) the concurrently measured, normalized, and remotely sensed signal $R_s/R_s(0.2 \text{ T})$ for a high mobility GaAs/AlGaAs specimen. Various colored traces correspond to the different power levels over the range $0 \leq P \leq 3.2$ mW. The blue upward arrows in (a) point out the inflections of the oscillatory resistance.

of the second maxima observed with increasing high magnetic field. The small peaks represent the two photon process, which will be discussed below.
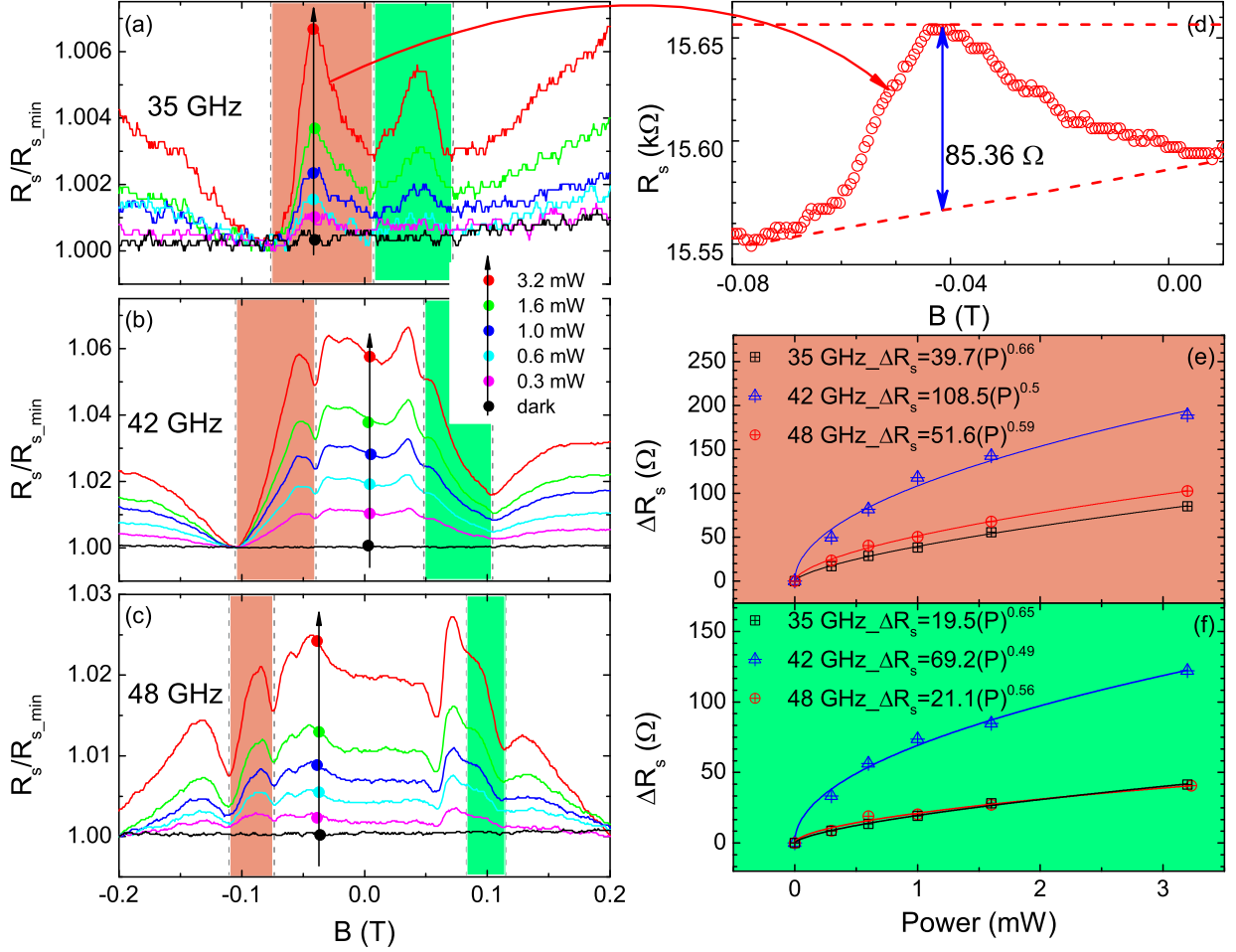
Figure 2.4. (a) The left column shows the power dependence of R_s vs. B under (a) 35 GHz, (b) 42 GHz and (c) 48 GHz microwave excitation. All R_s curves are normalized to their own lowest values.(d) illustrates the determination of the amplitude ΔR_s of the R_s oscillation at 3.2 mW power of 35 GHz in the brown area.The arrowed blue line indicates the ΔR_s associated with this oscillation. Panels (e) and (f) show plots of ΔR_s as functions of microwave power. Panel (e) corresponds to the oscillations in the brown shaded area in panel (a)-(c) and panel (f) corresponds to the green shaded area in panel (a)-(c). Different symbols indicate different frequencies: squares for 35 GHz, triangles for 42 GHz, and circles for 48 GHz. Power law functions are adopted to fit the solid lines to the symbols. The fit results are also given in panels (e) and (f).

Fig. 2.4 (a)-(c) examines the evolution of reflection oscillations with microwave power. Here R_s values are normalized to minima as $R_s(B)/R_{s\_min}$ since R_s signal is also sensitive to the heating produced by the incident microwaves. As microwave power increases from 0 to 3.2 mW, the oscillation amplitude of R_s becomes larger, but their locations on the abscissa do not change. Thereafter,

the amplitudes of the oscillations from different microwave power traces were evaluated without normalization. As indicated in Fig. 2.4 (d), the amplitudes were measured as the vertical height from the peak to the base line of one oscillation and plotted as a function of microwave power in Fig. 2.4 (e) and (f), respectively, for the oscillations at negative and positive magnetic fields. The power dependence of the R_s oscillation amplitude for all frequencies fits well with a power law function

$$\Delta R_s(P) = AP^\alpha \tag{2.3}$$

where A and α are fit parameters that vary with microwave frequency. Note that the α values of every frequency are close to 1/2. Also, the α values for each oscillation at positive and negative magnetic fields are almost the same: 0.66 (-B) and 0.65 (+B) for 35 GHZ; 0.5 (-B) and 0.49 (+B) for 42 GHz; and 0.59 (-B) and 0.56 (+B) for 48 GHz.
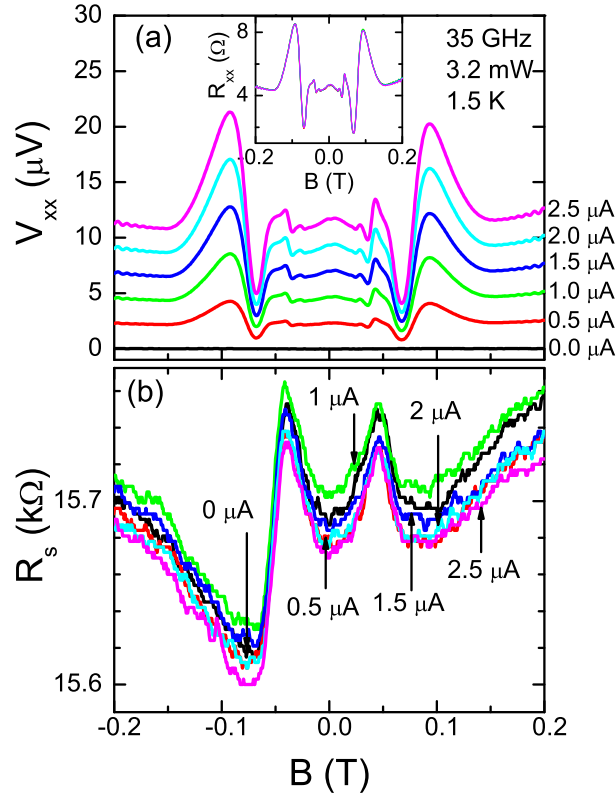
Figure 2.5. The diagonal voltage V_{xx} and the remote sensor resistance R_s are exhibited for a GaAs/AlGaAs specimen S1 under 35 GHz microwave excitation. The different color curves correspond to discrete applied currents, I, through the sample with $0 \leq I \leq 2.5$ μA. The same color code has been used in the top and bottom panels. The inset of (a) plots R_{xx} as a function of B. Curves for each applied current are overlapping.

Fig. 2.5 exhibit the current dependence of

$$V_{xx} = IR_{xx} \tag{2.4}$$

for R_s at 35 GHz and P=3.2 mW. Here, V_{xx} is plotted rather than R_{xx} because on the one hand V_{xx} is the actual measured term and on the other hand when current I is zero, R_{xx} is undefined by Ohms law. As shown in Fig. 2.5 (a), when the applied current decrease from 2.5 μA to 0 μA, the longitudinal voltage V_{xx} decreases proportionally as expected through Ohms law. Fig 2.5 (b) shows the concurrently measured sensor signal R_s. As the applied current in the sample reduced from 2.5 to 0 μA, the reflection signals of each current overlap each other, which means that the microwave reflection from 2DES does not change as the applied current in sample changed.
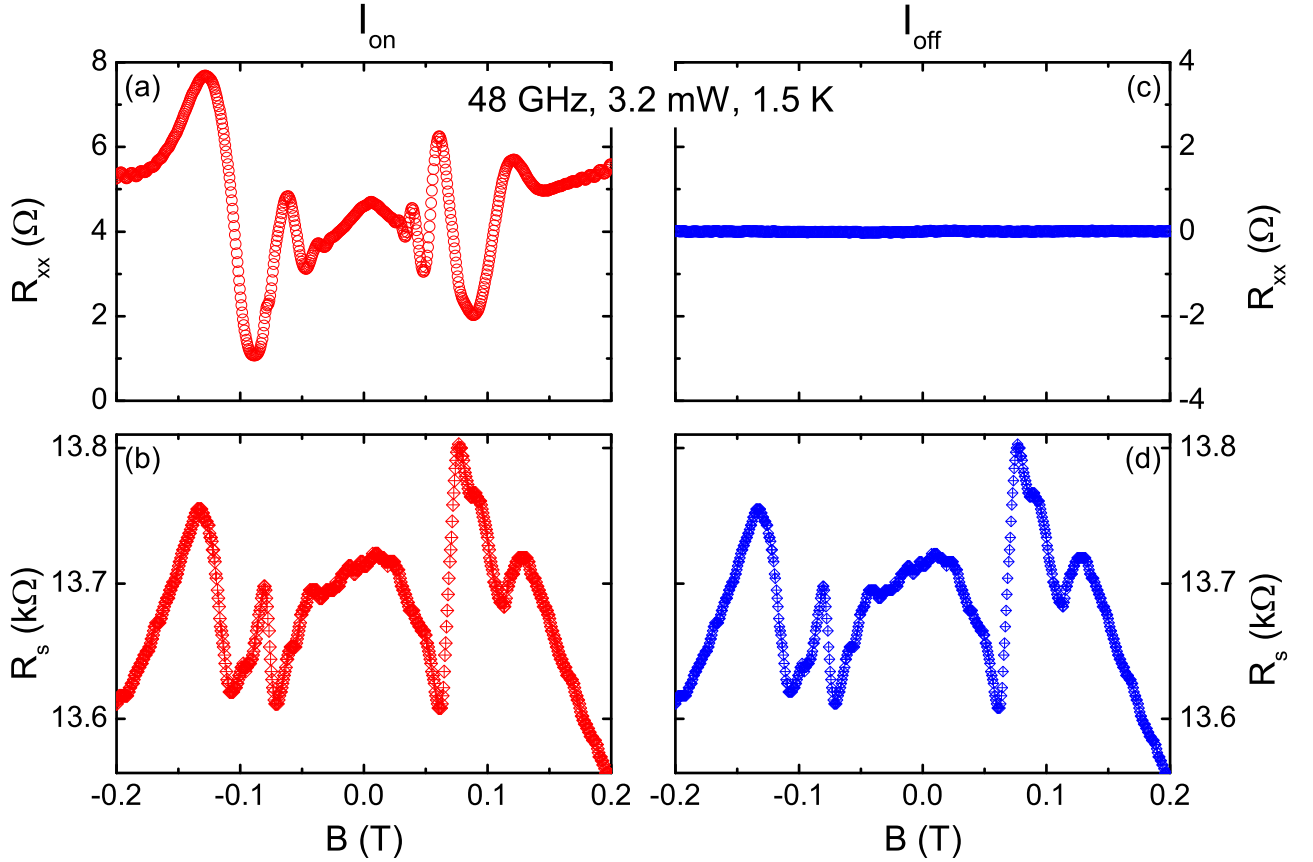
Figure 2.6. The diagonal voltage V_{xx} and the remotely sensed signal R_s for a GaAs/AlGaAs 2DES subjected to 48 GHz microwave excitation. In plots (a) and (b), the applied current is on. Plots (c) and (d) correspond to current off. Note that the R_s signal remains unchanged upon switching off the current through the specimen.

To convey this feature more clearly, Fig. 2.6 plots V_{xx} vs B and R_s vs B for the turned on applied current at 1 μA and the turned off applied current with 48 GHz and 3.2 mW microwave radiation. When the applied current is switched off, the V_{xx} vanishes; however the oscillations in R_s due to the microwave reflection from the photo excited 2DES persist even in the absence of the applied current. This indicates the existence of a reflective microwave induced response in the 2DES, which does not rely on the applied current through the 2DES.

Fig. 2.7 shows the microwave frequency dependence of the magneto-resistance of sample and sensor. The left column shows the longitudinal resistance R_{xx} vs B as microwave frequency increases from 35 GHz to 42 GHz to 48 GHz. As frequency increases, MRIMOs span a wider magnetic field regime. Such behavior is due to larger Landau level splitting, which is required to obtain energy commensurability as the photon energy hf increases. The right column shows the concurrently measured sensor signal R_s. Similar to R_{xx}, as the frequency increases, R_s oscillations also span a wider magnetic field range. Similar to MRIMOs, as the frequency increases, more oscillations appears in the R_s signal. For every R_s vs B trace, there is a step-like response in the vicinity of the starred location in Fig 2.7 right column. This feature of microwave reflection is similar to the electron absorption of microwaves reported by Inarrea *et. al.* [57].

Fig. 2.8 (a)-(c) shows R_{xx} and R_s as functions of B/f at 35 GHz, 42 GHz and 48 GHz. More MRIMOs reveal themselves in the R_{xx} vs B/f traces as frequency increases. For example, there are three MRIMOs appearing on each direction of magnetic field in the 35 GHz trace but there are four MRIMOs in the 48 GHz trace. Here, R_{xx} is plotted as a function of B/f, so MRIMOs do not shift positions on the abscissa as the frequency changes. Similar to R_{xx}, the turning points of R_s on the abscissa also do not shift with changing frequency. They are fixed within the regime of $2.3 \times 10^{-3} < B/f < 2.5 \times 10^{-3}$ T/GHz, which is slightly above the cyclotron resonance. In the regime where $|B/f| < 2.3 \times 10^{-3}$ T/GHz, the microwave energy is greater than the cyclotron resonance energy, and therefore radiation induced, inter-Landau-level transitions are allowed. Hence, the sensor signal starts to oscillate when radiation induced inter-Landau-level transitions are allowed in 2DES.

The displacement model [46] predicts maximum absorptions at the cyclotron resonance and its higher harmonics. As well, there are two photon assisted absorption peaks in the same simulation, Therefore, Fig. 2.9 plots the R_{xx} and R_s vs ω_c/ω, where ω_c is the electron cyclotron resonance
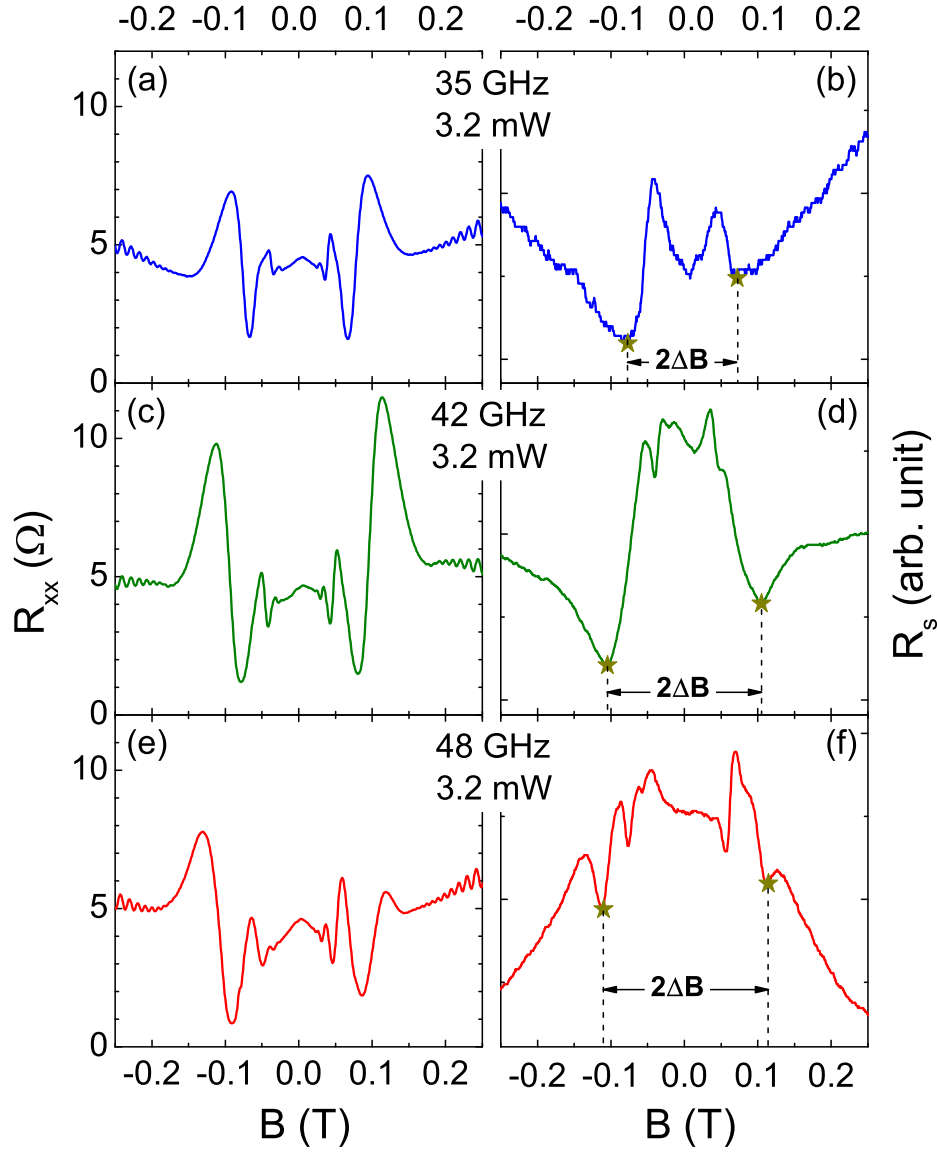
Figure 2.7. The left column shows the diagonal resistance, R_{xx}, vs. the magnetic field, B, for various microwave frequencies. The right column shows the corresponding sensor resistance, R_s, vs. B. From top to bottom, the microwave frequencies are 35 GHz, 42 GHz, and 48 GHz. Stars in the right column mark the last major valley in the R_s traces.
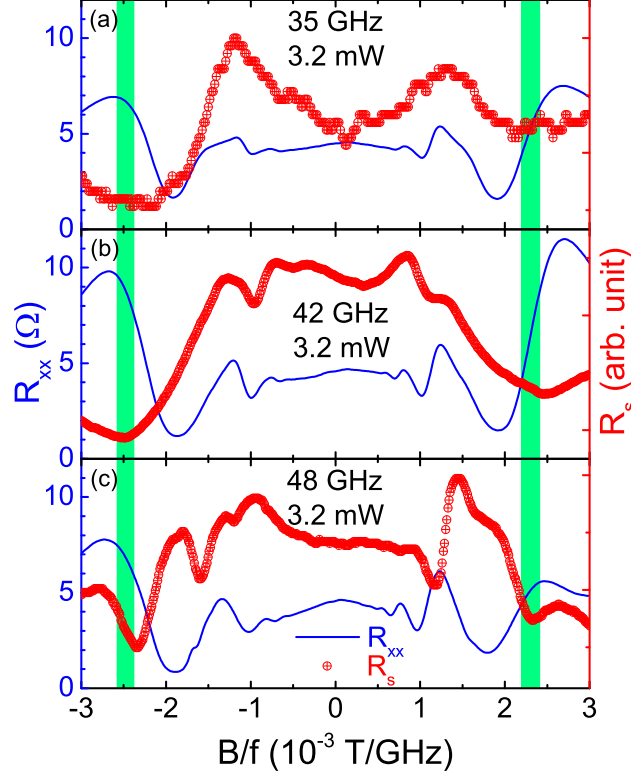
Figure 2.8. Panels (a) to (c) plot R_{xx} (left scale) and R_s (right scale) as functions of B/f for (a) 35 GHz, (b) 42 GHz and (c) 48 GHz microwave frequencies with 3.2 mW microwave power. Shadowed vertical bands mark the minima of the R_s traces.
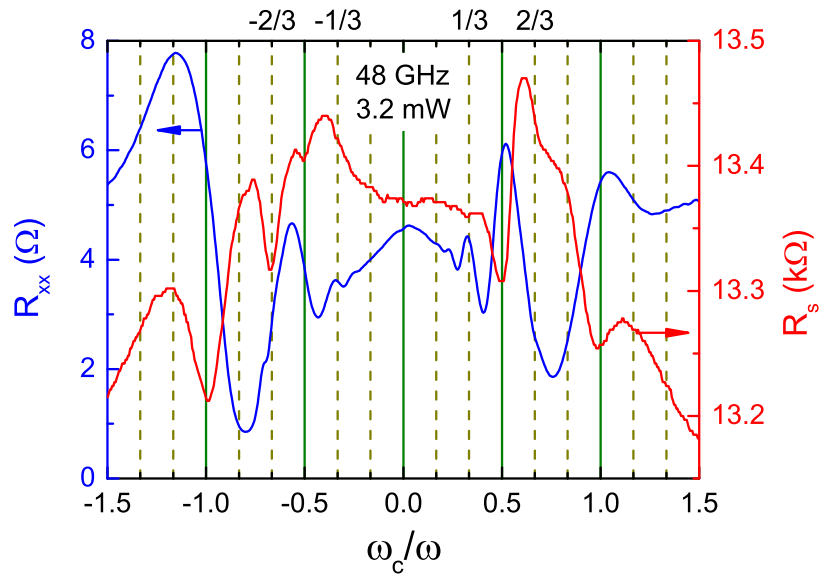
Figure 2.9. Longitudinal resistance R_{xx} of the high mobility GaAs/AlGaAs specimen with 48 GHz MW illumination. The red curve shows the concurrently measured carbon resistance R_s for the high mobility specimen. Here the variable on the abscissa is the ratio of cyclotron resonance frequency to microwave angular frequency ω_c/ω.

frequency and ω is the microwave angular frequency where

$$\omega = 2\pi f \tag{2.5}$$

in order to compare our results with unit of the cyclotron resonance. In Fig. 2.9, all R_s minima appear within

$$|\omega_c/\omega| < 1 \tag{2.6}$$

near

$$\omega = \pm j\omega_c, j = 1, 2 \tag{2.7}$$

and

$$2\omega = j\omega_c, j = 3 \tag{2.8}$$

These results clearly suggest that the maximum microwave reflection occurs at the cyclotron resonance and its second harmonic, which implies a microwave excited electron transition between integer times of LLs. Also, the $2\omega = j\omega_c$ feature implies the two-photon-excited electrons between integer LLs.

2.2.4 Discussion

As mentioned, there are many proposed mechanisms for the MRIMOs. For this discussion, we compare with mechanisms including the radiation-assisted, indirect, inter-Landau-level scattering by phonons and impurities (the displacement model) [44, 46, 49], a radiation-induced steady state non-equilibrium distribution (the inelastic model) [51], and the periodic motion of the electron orbit centers under irradiation (the radiation driven electron orbit model) [50, 57].

In the displacement model [44, 46, 49], microwave photo-excited electrons are scattered by impurities, and this gives rise to an additional current density due to the radiation. Here, the position dependent scattering rate is calculated using a generalization of Fermi's golden rule, and this is used to calculate the scattered current density, ΔJ_x, which depends on the initial and final average local density of states. Note that, ΔJ_x vanishes in zeroth order in the applied electric field. ΔJ_x to first order in the applied electric field, E_{dc}, is linear in E_{dc}. Thus, if $E_{dc} \to 0$, then

$\Delta J_x \to 0$. And therefore, naively, one does not expect an observable experimental effect in the limit of $E_{dc} \to 0$.
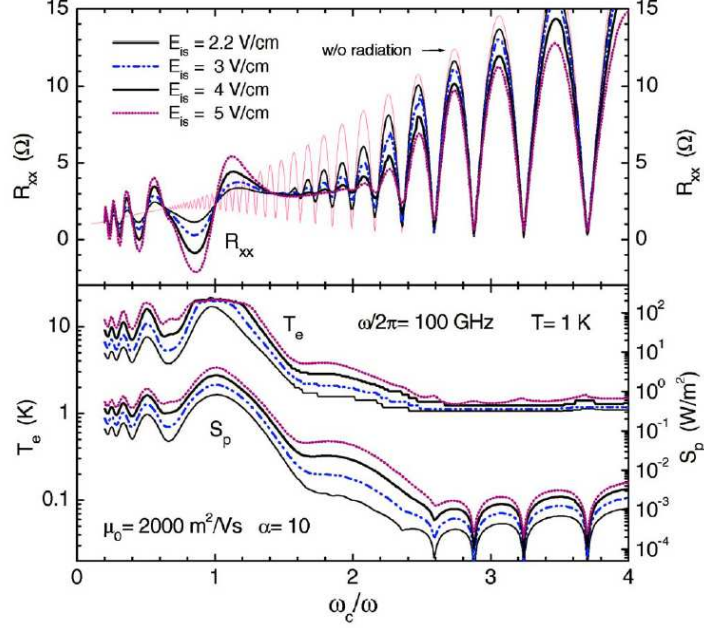
Figure 2.10. The magneto-resistivity R_{xx}, electron temperature T_e, and energy absorption rate S_p vs the ratio of cyclotron resonance frequency to microwave angular frequency of a GaAs-based 2DES with μ_0=2000 m^2/Vs mobility, subjected to 100-GHz linearly x-polarized incident high frequency fields $E_{is} \sin(\omega t)$ of four different strengths. (After Lei *et al.* [49])

In the displacement model [46, 49], Lei and Liu examined the interaction between electrons and the microwave field in the Faraday geometry, as the c.m. of the 2DES executes cyclotron motion. They asserted that, in the presence of impurity and phonon scattering, which couple the c.m. and relative motions, the microwave field affects the relative motion by allowing transitions between different states, leading to radiation-induced magnetoresistance oscillations. In subsequent work [49], they characterized the electron temperature in such a system by balancing the energy absorption from the radiation field with the energy dissipation to the lattice via the electron-phonon interaction, see Fig. 2.10. They suggest that oscillations in the energy absorption rate, S_p are correlated with resonant oscillations in the electron temperature. This will occur especially at frequencies

$$\omega = \pm j\omega_c \tag{2.9}$$

and

$$2\omega = j\omega_c \qquad (2.10)$$

, where S_p will attain its maxima, which is consistent with our observation in Fig. 2.9. Although the authors did not explicitly examine the variation of S_p in the limit of a vanishing applied electric field or current, it appears plausible that the energy absorption rate of the 2DES might be independent of whether or not an applied electric field or current exists in the specimen. If S_p continues to exhibit resonant oscillations even without an applied current or electric field, then it seems plausible that the reflected microwave power would follow the oscillatory S_p and also exhibit oscillations as seen in the experimental data here. Therefore, one might tentatively attribute the oscillations in the remotely sensed signal R_s to the oscillatory variation in the energy absorption rate of the microwave photo-excited 2DES and the concomitant change in the reflection.

The inelastic theory [51] for magneto-oscillations in the photo-conductivity of the 2DES, is governed by the microwave-induced change in the distribution function. Here, steady state microwave photo-excitation produces a change in the distribution function with oscillatory components that lead to oscillatory variations in the photo-conductivity, which are linear in the microwave power, see also ref. [30, 56]. These authors have asserted that this mechanism accounts for the dominant effect since, here the effect of the ac field on the distribution function is accumulated over the time scale τ_{in}, which is usually large compared to the single particle lifetime under typical experimental conditions. In the notation of this theory, since the photo-conductivity σ_{ph}, which determines the longitudinal current flowing in response to a dc electric field, ϵ_{dc}, in the presence of a microwave electric field $\epsilon_\omega \cos \omega t$, depends on ϵ_{dc}, this contribution is expected to disappear in the limit $\epsilon_{dc} \to 0$. A theory for quantum oscillations in the magneto-absorption has also been developed in this formalism. This theory suggests that quantum magneto-oscillations in the reflection coefficient ought to be much weaker than magneto-oscillations in the absorption, and therefore were not detected in some early experiments.

In the radiation driven electron orbit model [50, 57], one expects a periodic back- and forth-radiation driven motion of the electron orbits. Since such oscillatory motion of electron charge is, from the classical perspective, expected to produce radiation, such a reflection signal reported by R_s might be expected. A full theory of this has not yet been published. However, its simulation of

the microwave power dependency appears to be consistent with our results. This model claims that

$$R_{xx} \propto E_0 \tag{2.11}$$

where R_{xx} is the longitudinal resistance and E_0 is the amplitude of the microwave electric field. This model also asserts that

$$R_{xx} \propto \sqrt{P} \tag{2.12}$$

because the microwave power

$$P = \frac{1}{2} c_{GaAs} \epsilon_{GaAs} \epsilon_0 E_0^2 \tag{2.13}$$

where c_{GaAs} is the speed in light of GaAs and ϵ_{GaAs} is the dielectric constant of GaAs, and ϵ_0 is the dielectric constant in vacuum. This implies a resistivity-power exponent of $1/2$, which is similar to the experimental results shown in Fig. 2.4 (e) and (f). Moreover, the microwave absorption in this simulation reveals a sharp change in the microwave absorption of 2DES around the cyclotron resonance frequency, which is also consistent with our observations in Fig. 2.9.

2.3   Reflection measurements by the microwave power detector

2.3.1   Measurement details

The aim of this set of experiment is to use a different method to measure microwave reflection from 2DES. The samples measured here were still high mobility GaAs/AlGaAs heterostructures 2DES. Measurements were basically the same except for the reflection part. For the microwave reflection measurement we used a set-up schematically shown in Fig. 2.11 (a). A waveguide coupler was connected on the top of cylindrical waveguide. A microwave launcher was mounted on top of the coupler and a Hewlett Packard power detector was connected on the side of the coupler. In this way, we could both send microwaves down to samples and receive the microwave reflection from the power detector. The detectable frequency range of the power detector is between 33 GHz and 50 GHz, which matches the frequency range we were using to illuminate samples. Therefore, the signals concurrently measured here were the magneto-resistance, R_{xx}, in the sample and the microwave reflection, P_D, read by the microwave power meter.
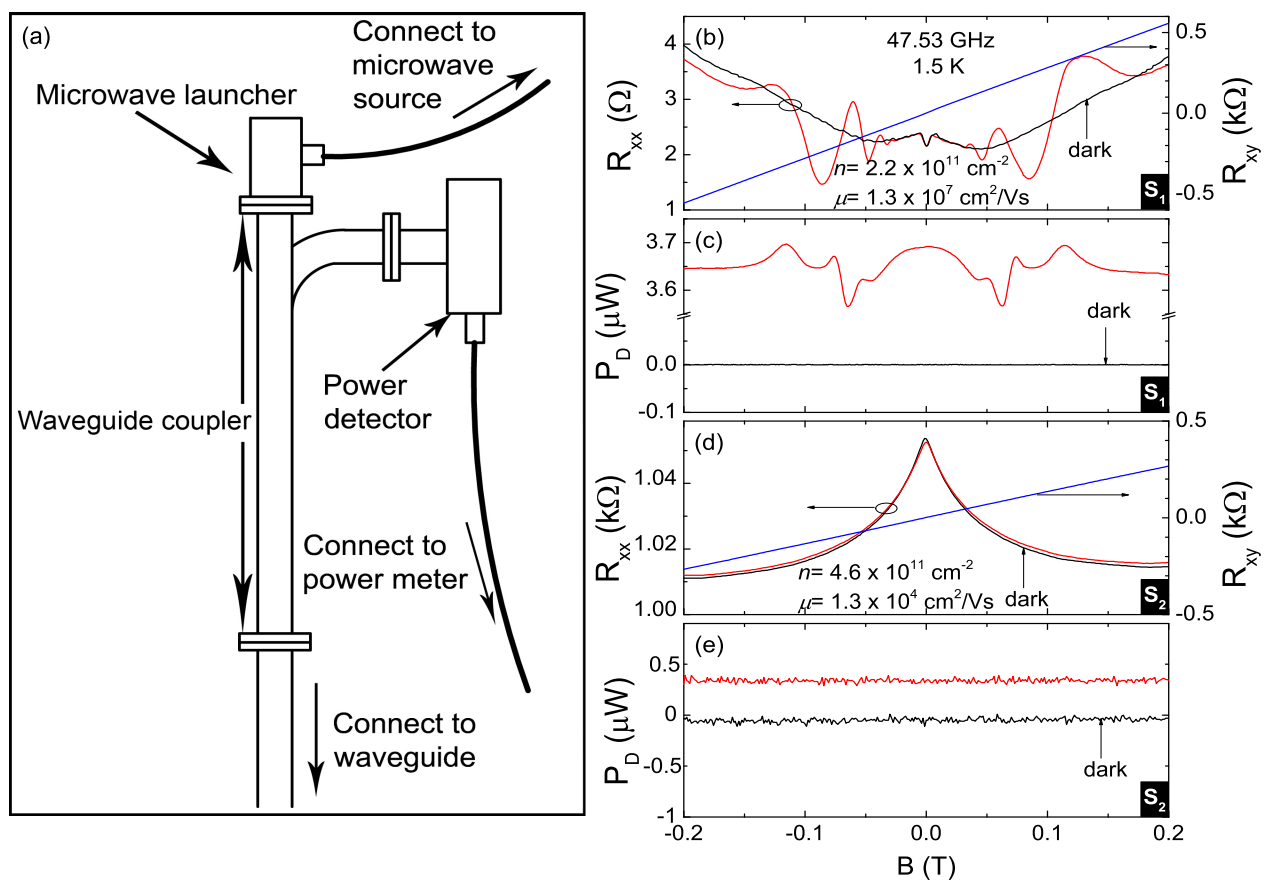
Figure 2.11. (a) A schematic of the measurement configuration shows the relative positions of microwave launcher, waveguide coupler and power detector. (b) Sample S1's longitudinal resistance (plot on left panel) and Hall resistance (plot on right panel) as functions of magnetic field. (c) Sample S1's power detector readings as functions of magnetic field. For (b) and (c) all red curves are signals with 47.53 GHz microwave illumination and all black curves are signals without microwave illumination (dark). (d) and (e) show the exact same measurement but on a low mobility sample S2.

2.3.2 Microwave reflection test of the microwave power meter

Fig. 2.11 (b) and (c) compare the longitudinal resistance R_{xx} and the concurrently measured detector reflection signal P_D of a high mobility sample S1. Carrier density and mobility at 1.5 K are specified in (b). Fig. 2.11 (b) shows without microwave illumination (dark), there are no MRIMOs in R_{xx}. While the magnetic field was sweeping, P_D was measured simultaneously as R_{xx}. Under the exact same conditions, the reflected power P_D formed a straight line at zero μW, which means there is no detectable microwave reflection. However, with 47.53 GHz microwave illumination, R_{xx} exhibited huge MRIMOs in the regime of -0.2$\leq B \leq$0.2 Tesla. In the same regime, P_D also exhibits obvious oscillations. The amplitude of P_D oscillations is as huge as 0.2 μW and the center of the amplitude is around 3.65 μW. From this preliminary result, we can conclude that the presence of microwaves is the exact factor that causes the oscillations both in R_{xx} and P_D. However, at this point we could not distinguish whether the P_D oscillations are generated by incident microwaves or microwave reflection from the 2DES. Therefore, we measured S2 with the exact same experiment set-up and under the exact same environment. Since it is known that MRIMOs strongly depend on the sample's mobility, a low mobility sample should not exhibit any MRIMOs. Fig. 2.11 (d) and (e) show that no matter with or without microwave illumination, R_{xx} does not exhibit MRIMOs in the regime of -0.2$\leq B \leq$ 0.2 Tesla. Similarly, the concurrent measured P_D signal exhibits only a flat line at around 0.4 μW without any oscillation. This result proves that the oscillations in P_D are nothing else but the reflection from the high mobility 2DES sample and they are correlated with high mobility sample's MRIMOs.

2.3.3 Power meter results

Fig. 2.12 shows the 42.53 GHz microwave power (microwave source power) P_i dependence upon magneto-resistance measurement of the high mobility sample S1. Fig. 2.12 (a) shows the diagonal resistance traces as microwave power changes from 4 mW to 0 mW. It is clear that as incident microwave power decreases, the amplitude of MRIMOs decreases. In Fig. 2.12 (b) to (f), the amplitude of the P_D oscillations also decreases as microwave power decreases. But the P_D oscillations still occur at the same magnetic field levels as microwave power varies. Next we examine the amplitude change of the oscillations in both R_{xx} and P_D. Because both types of oscillations are
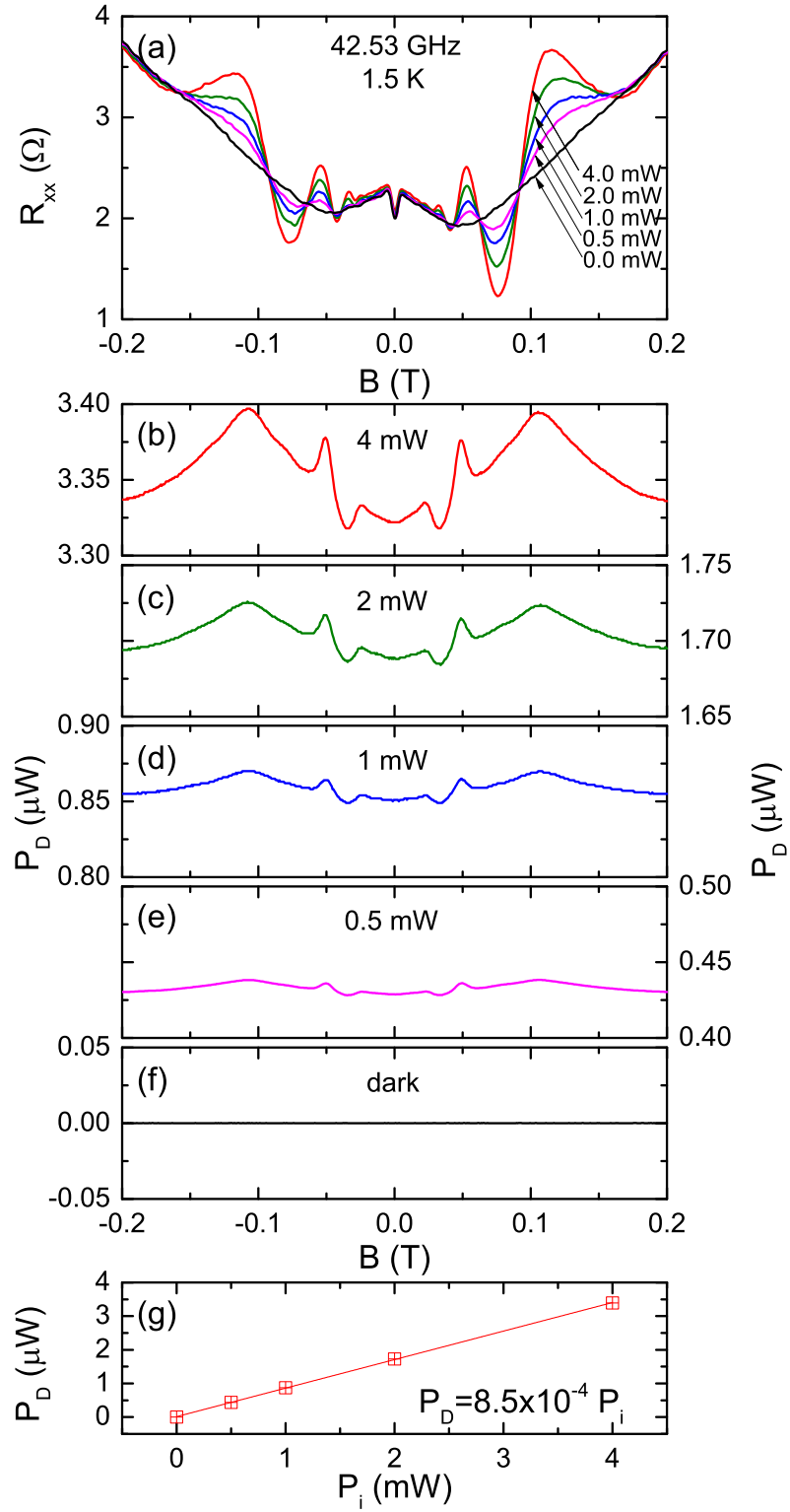
Figure 2.12. (a) Longitudinal resistance as functions of magnetic field with 42.53 GHz microwave illumination. Different colour curves show signals with different power. (b) to (f) Microwave reflection signals as functions of magnetic field under illumination of 42.53 GHz microwaves with power (b) 4 mW, (c) 2 mW, (d) 1 mW, (e) 0.5 mW and (f) 0 mW. (g) Amplitude of the first right maxima P_D as a function of microwave source power.

symmetric with respect to ordinate, the amplitudes of the first peaks from right side were picked from amplitude of each microwave power were plotted as function of microwave power P_i in Fig. 2.12 (g). The microwave power dependence of P_D indicates a linear relation between P_D and P_i.
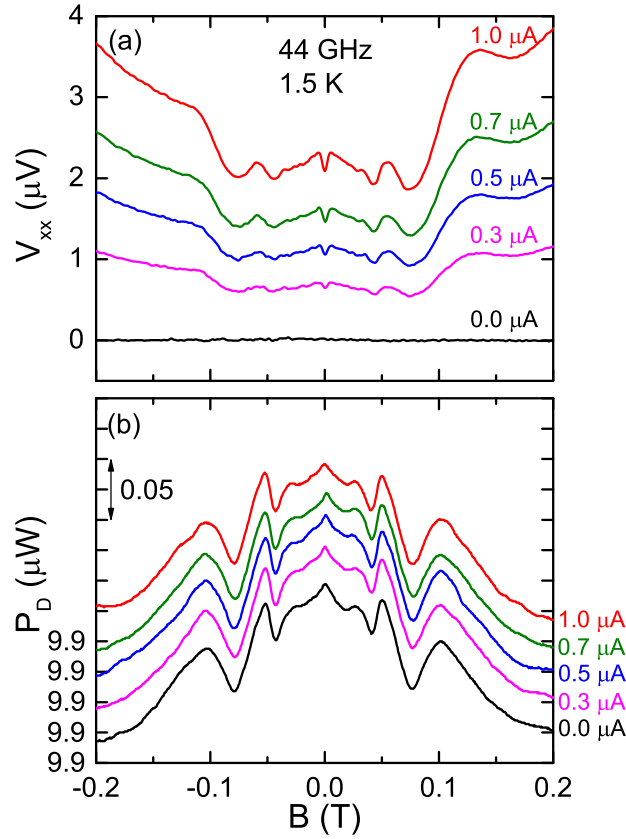
Figure 2.13. (a) V_{xx} as a function magnetic field with 44 GHz microwave illumination. Different curves indicate different driven current through sample. The applied currents are, from top to bottom: 1.0 μA, 0.7 μA, 0.5 μA, 0.3 μA and 0 μA. (b) A stack plot of P_D as a function of magnetic field under the same conditions as (a). All curves in (b) are shifted relative to a minimum at 9.9 μW. The double arrow bar shows the scale on the ordinate.

Fig. 2.13 examines the role of the applied current in the observed effects in R_{xx} and the reflection signal, P_D. Here, the measurements were carried out with 44 GHz microwave illumination at a constant microwave power P_i=4 mW. Here V_{xx} has been plotted rather than R_{xx} because R_{xx} is undefined when $I = 0$ μA. As the applied current, I, is gradually decreased from 1.0 μA to 0 μA, the diagonal voltage V_{xx} decreases proportionally, see Fig. 2.13 (a), as expected by the relation $V_{xx} = IR_{xx}$. Note also that the phase of oscillations in the V_{xx} signal does not change with the change in the current. Fig. 2.13 (b) shows a stack plot of the concurrently measured reflection

signal P_D at the same currents, I. All curves were shifted and stacked in order to identify each one clearly. Here, note that a change in the applied current does not make any systematic change in the P_D signal. As mentioned previously, the B- range of the P_D response spans the same domain as that for the oscillations in V_{xx} that are seen in Fig. 2.13 (a).

2.3.4 Discussion

The main features of the exhibited results are: a) Microwave reflection oscillations (MROs) are associated with the MRIMOs in 2DES. b) The MROs amplitudes are linearly dependent on the microwave power, which is different from the power dependency of the MRIMOs amplitudes. c) Same as MRIMOs, MROs do shift as microwave frequency varies. d) MROs are independent of the applied current.

Our MROs observations totally contradict the prediction in the previous literature [31] that microwave reflection could hardly be observed in quantum oscillations. In their paper Fedorych *et al.* considered the inverted momentum relaxation time τ_{tr}^{-1} as zero when sample mobility is relatively high, and in their experiment the mobility of 2DES was 10^7 cm^2/Vs. They found that, the oscillatory term $\cos(2eE/\omega_c)$ only shows up in the absorption coefficient but not in the reflection or transmission coefficients. However, in our experiment the sample mobility at 1.5 K was 1.3×10^7 cm^2/Vs, which is even a little higher than the value reported in the literature, and we did observe quantum oscillations in the microwave reflection. This means that there is still an oscillatory part in the reflection coefficient.

Moreover, microwave reflection does not change at all with applied current change. This indicates that the MROs are the result of electron transitions between Landau Levels subject to microwave radiation. As long as the microwave power, frequency and Landau Level quantization do not change, the electron transitions will be the same.

2.4 Conclusion

In conclusion, the magnetoresistive response of the microwave photo-excited GaAs/AlGaAs 2DES has been compared with the concurrent microwave reflection from the 2DES. The experimental results indicate a strong correlation between the observed features in the two types of

measurements. We have also observed that oscillatory features in the remotely sensed reflection signal exhibit a non-linear amplitude variation with the microwave power, similar to the power-law type variation reported for the oscillatory diagonal resistance associated with MRIMOs. Interestingly, the character of the reflection signal remains unchanged even when the current is switched off in the GaAs/AlGaAs Hall bar specimen. The results suggest that the 2DES is microwave active even in the absence of an applied current.

Chapter 3

COMBINED STUDY OF MICROWAVE-POWER AND LINEAR-POLARIZATION DEPENDENCE OF MRIMOS

3.1 Introduction

During the many years of MRIMOs study, many aspects of MRIMOs have been discovered. There were studies about the amplitude of MRIMOs. It was found that radiation power [30], linear polarization direction [32, 34], angle between magnetic field and sample normal [18] and the current through sample [14] are the factors that control the amplitude. There were also studies about MRIMOs period and phase [10, 29]. Period was found to be dependent on the radiation frequency and it is periodic about $1/B$. There is a 1/4-cycle-shift found to be exist on the phase of MRIMOs. All these dependencies of MRIMOs have been examined by different experiments and theories. But there are still some open questions. Two important ones are the microwave power dependence and radiation linear polarization dependence of MRIMOs. In the microwave power dependence, there were experiments results [30] that indicated a non-linear relation between the amplitude of MRIMOs and the microwave power. The radiation driven electron orbit model [56] has also confirmed this non-linear relation from a theoretical aspect, while the inelastic model [51] suggests a linear relation. About the role of microwave polarization in MRIMOs, the displacement model [64] and the radiation driven electron orbital model [68] suggested the MRIMOs amplitude depends on linear polarization angle, while inelastic model [51] indicated an independent relation between MRIMOs and linear polarization angle. On the other hand, one set of experiments [21] indicate MRIMOs are independent of the polarization orientation for both linearly and circularly polarized microwaves, while another set of experimental results [32, 34] reveal that the amplitude of MRIMOs depend on the polarization angle of linearly polarized microwaves. As well, this set of experiments [34] demonstrated a sinusoidal relation between longitudinal resistance R_{xx} and linear polarization angle θ

$$R_{xx}(\theta) = A \pm C \cos^2(\theta - \theta_0) \tag{3.1}$$

where $A, C, and \theta_0$ are constants. Moreover, this work found that at high radiation intensities, the previously stated relation suffers a deviation and no longer follows a cosine square rule. This result indicated that the radiation intensity does affect the polarization angle dependence. In order to understand the role of microwave power in the linear polarization dependence, a combined study of microwave-power and linear-polarization dependence was carried out.

3.2 Microwave power and polarization measurement details

The high mobility GaAs/AlGaAs heterojunction samples measured here were fabricated in the same way as stated in the previous chapter. Basic low temperature, low noise, magneto-transport measurements here are the same as the previous chapter. A commercially available microwave synthesizer provided the microwave excitation, and the microwave power at the source was changed at 1 dBm increments between 0 and 20 dBm. The linear-polarization angle, which is defined as the angle between the long axis of the Hall bar and the microwave antenna in the microwave launcher, see Fig. 3.1(a), was changed by rotating the microwave launcher outside the cryostat. The results reported here are characteristic of the power and polarization-angle dependence over the range from 30 to 50 GHz. However, we focus here on the results at the frequencies of 33.62 GHz and 45.2 GHz, since so many plots need to be exhibited to establish the overall behavior even at one frequency.

3.3 Results

3.3.1 Low microwave power results

Fig. 3.1 (b) shows our magnetoresistance measurements with magnetic field sweep and under 33.62 GHz microwave illumination. Photo-excited (w/ MW) and dark (w/o MW) diagonal magneto resistance R_{xx} and Hall resistance were obtained from this sweep. Pronounced MRIMOs shows up on both sides of B field in the photo-excited curve. The peaks and valleys of MRIMOs here are labeled by dash lines as $P1-$, $V1-$, $V1+$ and $P1+$. Here P (V) means peak (Valley) resistance, 1 means the first peak or valley from the high magnetic side, and plus or minus means the positive or negative of magnetic field. Since the labeled magnetic fields yield the maximum R_{xx} deviation from the dark curve, we shall examine the power dependence and polarization dependence at the associated four fixed B fields.
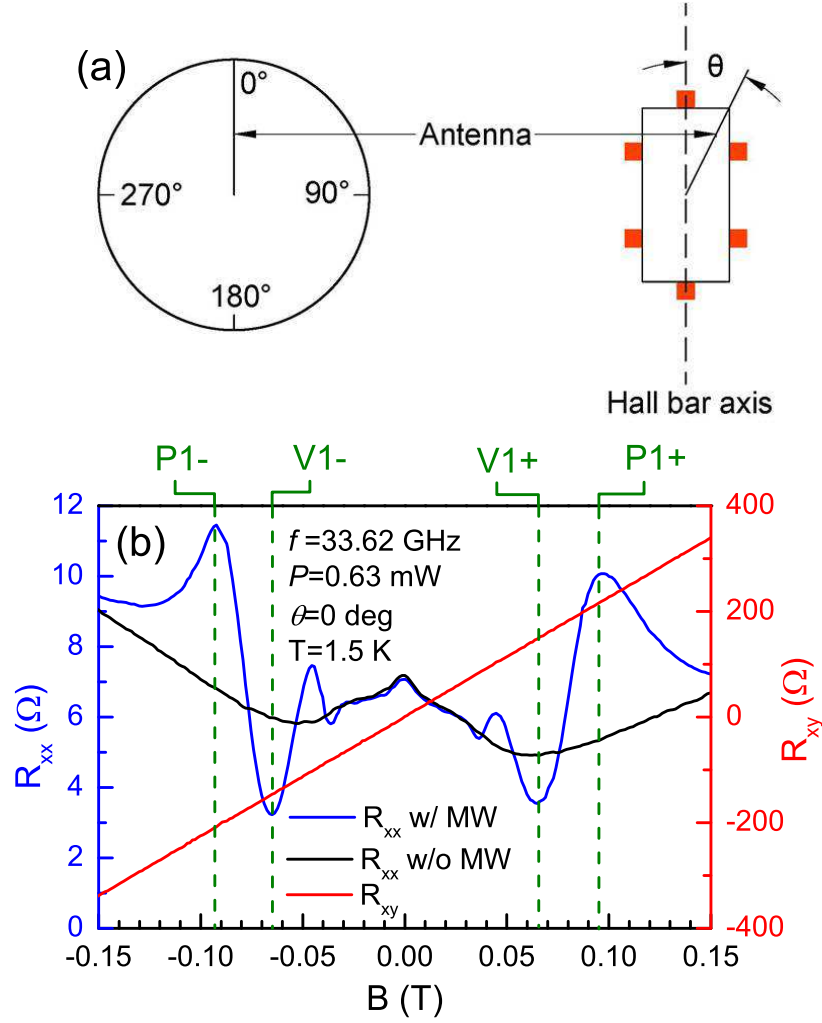
Figure 3.1. (a) is a sketch of the polarization orientation in the magnetotransport measurement. Here, the antenna and the microwave launcher rotate clockwise with respect to the long axis of Hall bar sample to set the polarization angle θ. (b) Diagonal resistance R_{xx} (left ordinate) and Hall resistance (right ordinate) versus the magnetic field B without (black curve) and with (red- and blue- curves) microwave photo-excitation at 33.62 GHz and $T = 1.5$ K. The polarization angle, θ, is zero. Symbols in green at the top abscissa mark the magnetic fields of some of the peaks and valleys of the oscillatory magnetoresistance.
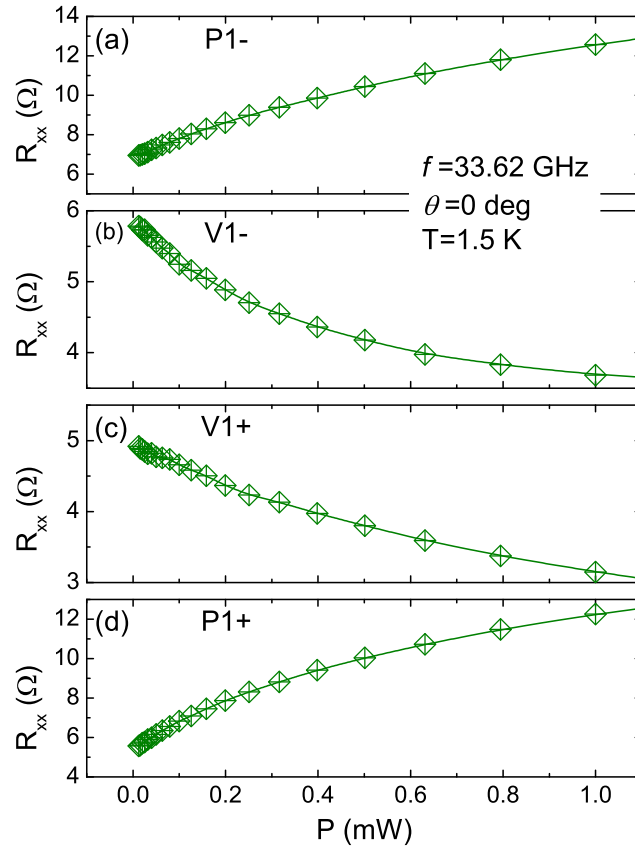
Figure 3.2. Microwave power dependence of magneto-resistance at extrema magnetic fields. Panels (a)- (d) show the R_{xx} as a function of the microwave power, P, at these peaks and valleys as follows: (a) P1-, (b) V1-, (c) V1+ and (d) P1+.

Fig. 3.2 exhibits R_{xx} as a function of microwave power P at the earlier mentioned four magnetic fields. Note here the unit of microwave power has been changed from dBm to mW for the sake of expressing power on a linear scale. As well, the power sweep region here was from 0 to 1 mW. Fig. 3.2 (a) and (d) exhibit the power dependence at the peaks of oscillatory resistance, so that R_{xx} increases as power increases. Similarly, Fig. 3.2 (b) and (c) exhibit power dependence at the valleys of oscillatory resistance, and R_{xx} drops as power increases. Here, neither the increase of R_{xx} with P nor the decrease of R_{xx} with P is linear with respect to microwave power.
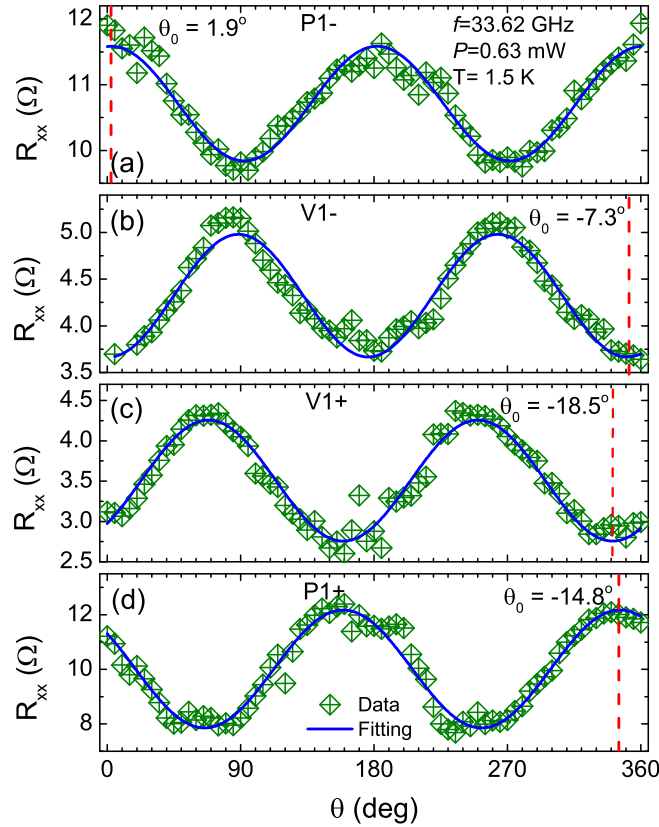
Figure 3.3. (a) to (d) R_{xx} versus the polarization angle θ at the magnetic fields corresponding to the oscillatory extrema (P1-, V1-, V1+, and P1+) marked in Fig. 3.1(b). Here, the microwave frequency is 33.62 GHz and power is 0.63 mW. Blue lines are the fit curves to $R_{xx}(\theta) = A \pm C \cos^2(\theta - \theta_0)$. Here, in the "$\pm$" sign, the "+" sign applies for (a) and (d), while the "-" sign applies for (b) and (c). Vertical dashed lines mark the polarization phase shift angle, θ_0, for each fit curve.

The R_{xx} vs P measurements at the four magnetic fields were carried out at a number of linear polarization angles over the range from 0° to 360° with a 10° increments. Fig. 3.3 summarizes the extracted angular dependence at a fixed source power, P=0.63 mW. From Fig. 3.3 (a) to (d), R_{xx} vs θ curves vary sinusoidally with θ. Actually, the data curves follow the fitting function [34]

$R_{xx}(\theta) = A \pm C \cos^2(\theta - \theta_0)$ indicated by blue curves in the figure. Both data and fitting results confirm a π period as mentioned in [34]. Further, the phase shifts for the four curves are $\theta_0 = 1.9°$ for $P1-$, $\theta_0 = -7.3°$ for $V1-$, $\theta_0 = -18.5°$ for $V1+$ and $\theta_0 = -14.8°$ for $P1+$. These extracted phase shifts indicate finite phase changes within 20°.
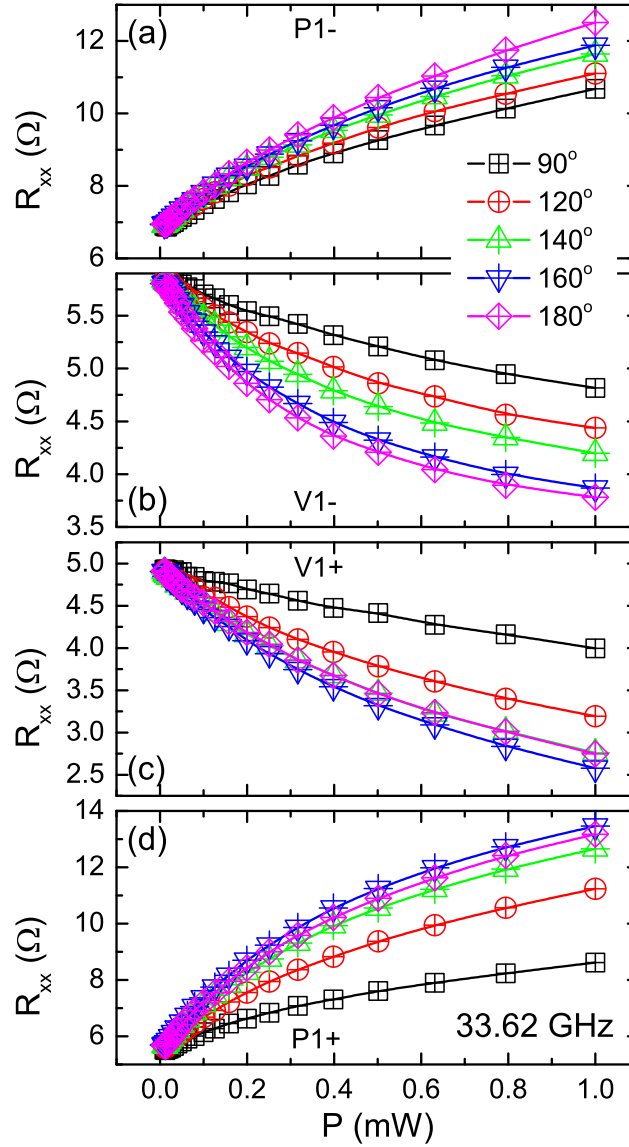
Figure 3.4. (a) - (d), the diagonal resistance R_{xx} is plotted versus the microwave power P at various fixed polarization angles for the R_{xx} extrema as follows: (a)P1-, (b)V1-, (c)V1+ and (d)P1+. The different symbols stand for different polarization angles from 90° to 180°, as indicated.

Fig. 3.4 shows the fixed magnetic field relation R_{xx} vs P at different discrete polarization angles. The magnetic field was fixed at the peaks and valleys of MRIMOs. The power dependence of each R_{xx} curve shows non-linear relation between R_{xx} and incident microwave power: different

angle curves start at the same point at 0 mW and start to split as P increases and these non-linear curves are different for different polarization angles. A closer examination suggests, however, that all the curves in Fig. 3.4 (a) to (d) follow a similar trend. Therefore, we utilize a power scaling factor P_s to normalize the different curves in each figure to the same curve.
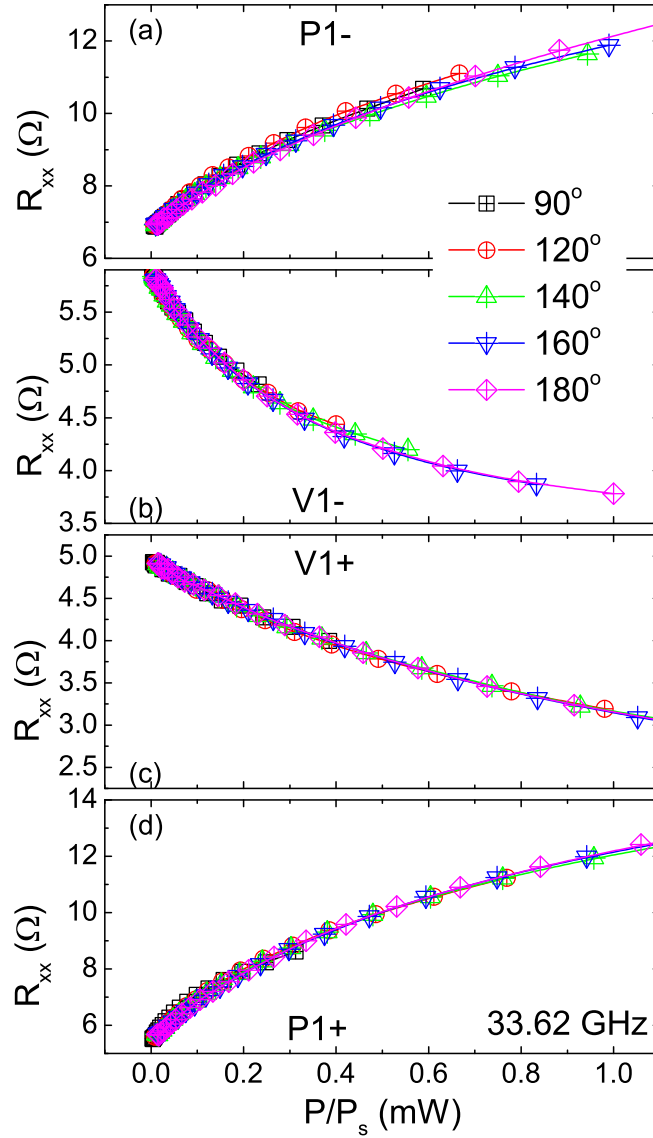
Figure 3.5. Plots (a) to (d) show the extremal R_{xx} versus P/P_s. Here, P_s is a polarization angle dependent power scaling factor that normalizes curves in Fig. 3.4 at different polarization angles to the same curve.

Fig. 3.5 (a) to (d) shows the curves after normalization. The curves in each panel of Fig. 3.4 could be normalized to the same curve by dividing their x axis by a polarization-angle dependent power scaling factor, $P_s(\theta)$. These power scaling factors depend on both magnetic field and polar-

ization angle. We found the power scaling factor exhibits simple behavior as the polarization angle changes as Fig 3.6 shows.
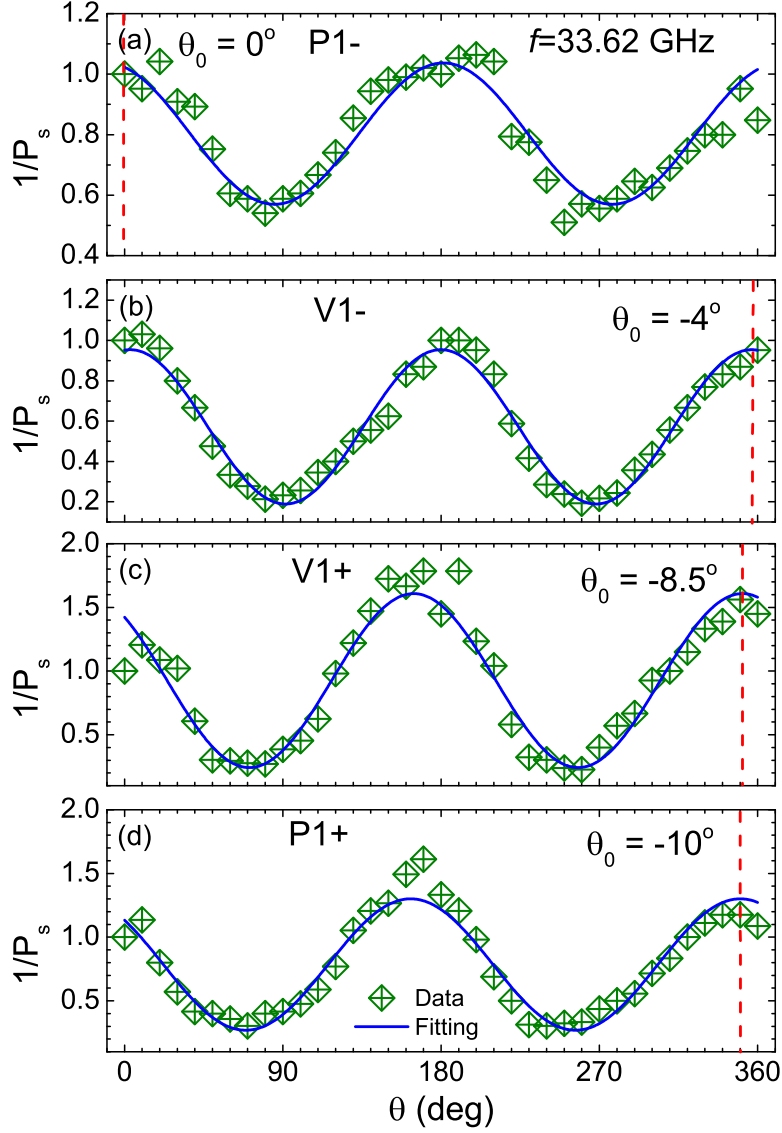
Figure 3.6. (a) The inverse power scaling factor, $1/P_s$, is plotted as a function of linear microwave polarization angle θ at the oscillatory magnetoresistance extrema: (a)P1-, (b)V1-, (c)V1+ and (d)P1+. Red curves represent the fit utilizing $1/P_s(\theta) = A + C\cos^2(\theta - \theta_0)$. Vertical dashed lines indicate the polarization phase shift angle, θ_0, obtained from the fit.

Fig. 3.6 shows the reciprocal power scaling factor $1/P_s$ plotted as a function of polarization angle θ for the fixed extreme magnetic fields. The factor $1/P_s$ varies sinusoidally with the polarization

angle θ and it also follows a function of the form

$$P_s(\theta) = A + C \cos^2(\theta - \theta_0) \tag{3.2}$$

Please note that, there is a difference between this fitting and the one used to fit R_{xx} vs θ because here both the peaks and the valleys in the oscillatory magnetoresistance show a + sign between the constant A and $C cos^2(\theta - \theta_0)$, while for the other one the + sign appears for oscillatory magnetoresistance maxima and the - sign appears for minima.

3.3.2 High microwave power results

In the previous results, there is no obvious curve deviation in the polarization angle dependence, R_{xx} vs θ, since the microwave power was maximally 1 mW, which is not too high to make a deviation. However, we made the same measurement in another sample by ramping the microwave power up to 4 mW, which is strong enough to introduce deviations in the polarization angle dependence. As Fig. 3.7 (a) shows, the measurement method is exactly the same as for the previous sample. Microwave power and polarization angle can be continuously changed. Fig. 3.7 (b) shows the R_{xx} measurement with sweeping magnetic field, from which the extrema magnetic field levels could be selected as $P1-$, $V1-$, $P2-$, $P2+$, $V1+$ and $P1+$. Fig. 3.7 (c) shows the deviation of the R_{xx} vs θ curve at high microwave power radiation at $P2+$ magnetic field. The blue scattered points show the measurement with 0.5 mW microwave power radiation, and this curve could be well fitted with $R_{xx}(\theta) = A \pm C \cos^2(\theta - \theta_0)$, which is shown in the blue curve. However, with 4 mW microwave power radiation, the R_{xx} vs θ curve (red points) start to deviate from the cosine square function (red line). The minima became sharper and maxima became broader.

To demonstrate the evolution of R_{xx} vs θ curve as a function of microwave power, color contour plots are presented in Fig. 3.8. The x axis represents the linear polarization angle, θ, and the y axis represents the microwave power, P. Color scales represent the numerical values of diagonal resistance R_{xx}. Brighter color indicates a higher R_{xx} value and a darker color indicates a lower one. Color scales are shown on the right side of each plot. For each plot the phase shift angle θ_0 is the same, approximately 30°. Here phase shift does not depend on the extrema or magnetic field. The gradient change in the color clearly shows a monotonically increasing of R_{xx} for $P1-$, $P2-$, $P2+$,
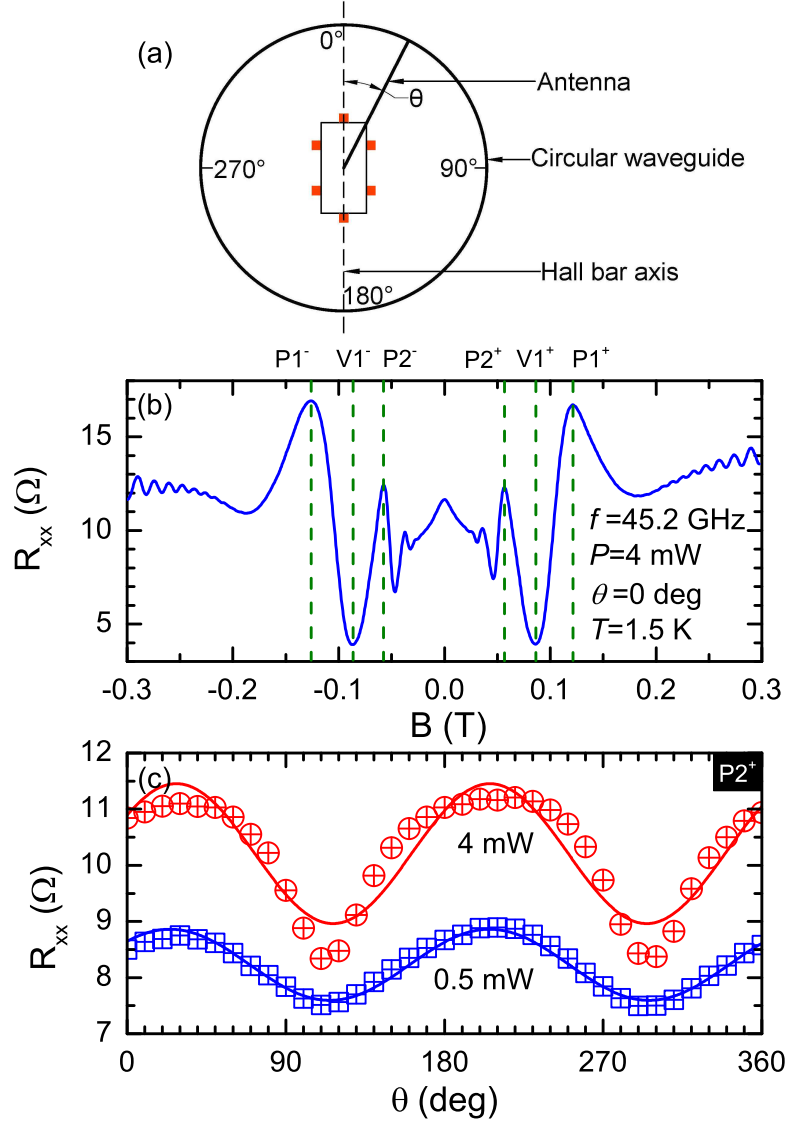
Figure 3.7. (a) A sketch of the polarization orientation in the magnetotransport measurement. Here, the antenna and the microwave launcher rotate clockwise with respect to the long axis of Hall bar sample to set the polarization angle θ. (b) Diagonal resistance R_{xx} versus the magnetic field B with microwave photo-excitation at 45.2 GHz and $T = 1.5$ K. The polarization angle, θ, is zero. Symbols, i.e., P1$^-$, V1$^-$, etc., at the top abscissa mark the magnetic fields of some of the peaks and valleys of the oscillatory magnetoresistance. (c) Daigonal resistance R_{xx} vs polarization angle θ at the P2$^+$ magnetic field with 4 mW (top red curve) and 0.5 mW (bottom blue curve) microwave illumination. Scattered points represent the experimental data and solid curves are fits utilizing the equation $R_{xx}(\theta) = A \pm C \cos^2(\theta - \theta_0)$.
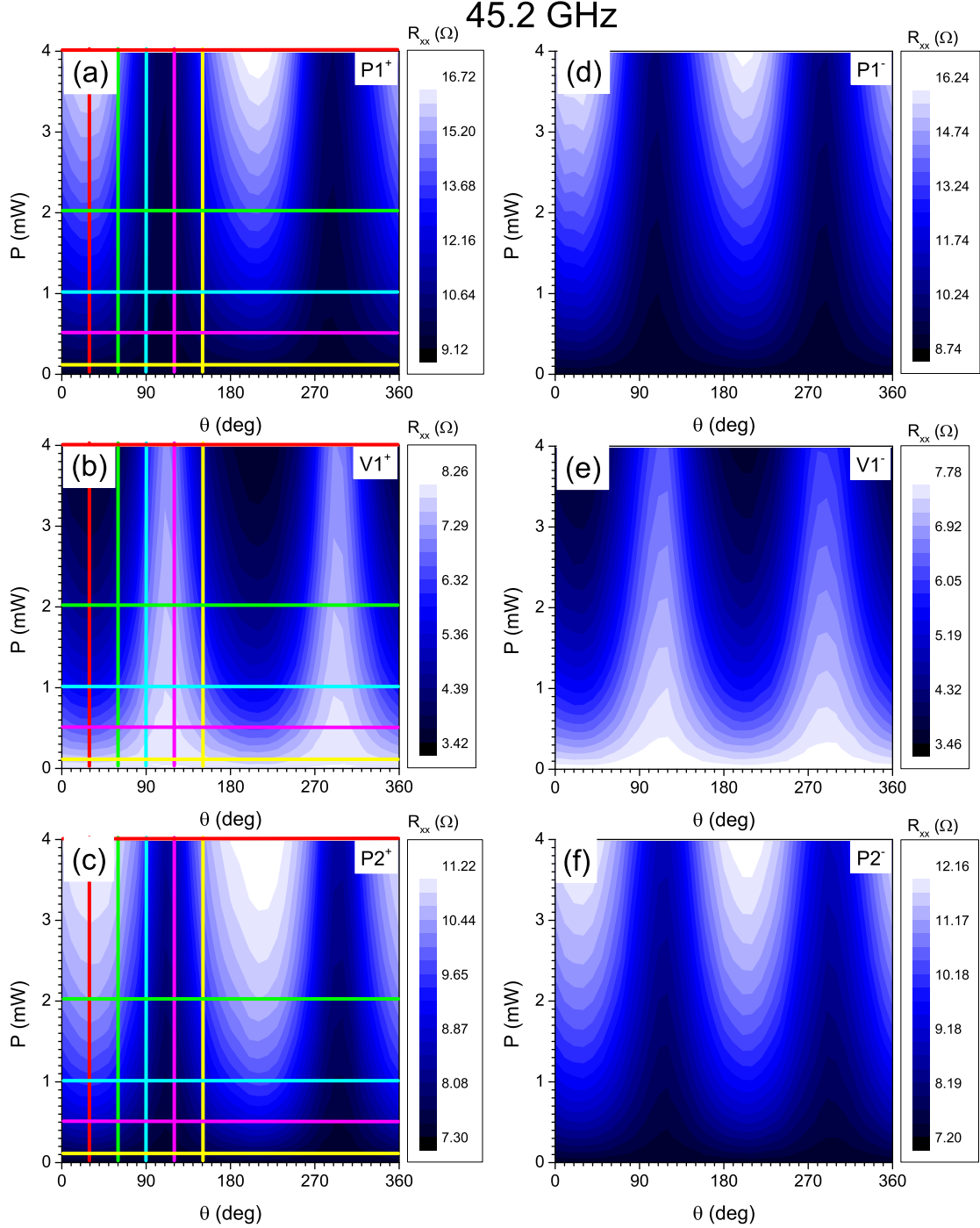
Figure 3.8. Color contour plots of diagonal resistance R_{xx} as a function of both microwave power (ordinates) and polarization angle (abscissas) at $f = 45.2$ GHz and at the magnetic field corresponding to (a) P1$^-$, (b) V1$^-$, (c) P2$^-$, (d) P1$^+$, (e) V1$^+$ and (f) P2$^+$. R_{xx} values are indicated by the color scales on the right side of each figure. Vertical solid lines in each figure indicate the polarization angles, at which R_{xx} vs P profile curves are shown in Fig. 3.9 (a)-(c). Horizontal lines in each figure indicate the power levels, at which R_{xx} vs θ profile curves are shown in Fig. 3.9 (d)-(f).

and $P1+$ and monotonically decreasing for$V1-$ and $V1+$ as microwave power increases. At fixed microwave power, R_{xx} changes periodically with θ. The vertical lines in the color plots indicate certain selected discrete microwave polarization angles from $0°$ to $150°$. R_{xx} is plotted vs P at these selected polarization angles in the left column of Fig. 3.9. The horizontal lines in the color plots indicate discrete microwave powers from 0.1mW to 4mW. Extracted R_{xx} vs θ at these P are shown in the right column of Fig. 3.9.

In the left column of Fig. 3.9, R_{xx} vs P curves for different polarization angles initiate from the same point at 0 mW but start to separate with increasing P. For $P1+$ and $P2+$, R_{xx} increases as the power increases and R_{xx} decreases as power increases at $V1+$. But the change in R_{xx} with P is non-linear. In the right column of Fig. 3.9, the plots show the deviation from simple sinusoidal behavior with increasing microwave power. Here for $P1+$ and $P2+$, the valleys become sharper and peaks become broader as microwave power increases, while for $V1+$ the peaks become sharper and valleys become broader as microwave power increases. Comparing the deviation from sinusoidal behavior for $P1+$ and $P2+$, the deviation is more obvious in $P2+$, which suggests the R_{xx} vs θ line shape evolution with microwave power becomes more pronounced at lower magnetic fields. Jointly consider the two columns in Fig. 3.9, although R_{xx} either increases (for $P1+$ and $P2+$) or decreases (for $V1+$) as microwave power increases, the rate of change of R_{xx} with P are different as Fig. 3.9 (a)-(c) show. It appears that the different non-linearity at different polarization angles is the main cause for the deviation of R_{xx} vs θ curves from simple sinusoidal at high microwave powers.

3.4   Discussion

The above mentioned results indicate: (a) the magneto-resistance R_{xx} is non-linearly related to the microwave power P. (b) The peak or valley magneto-resistance is a cosine square function of linear microwave polarization angle θ, i.e., $R_{xx}(\theta) = A \pm C \cos^2(\theta - \theta_0)$. (c) The R_{xx} vs P traces at different polarization angles for a given extremum look dissimilar at first sight, but they are really just manifestations of the same functional shape because the R_{xx} vs P curves for different polarization angles can be normalized by dividing with a power scaling factor P_s. Remarkably, this scaling factor also follows a cosine square function of linear microwave polarization angle. (d) Microwave power and linear polarization angle both influence the oscillatory R_{xx} in the high
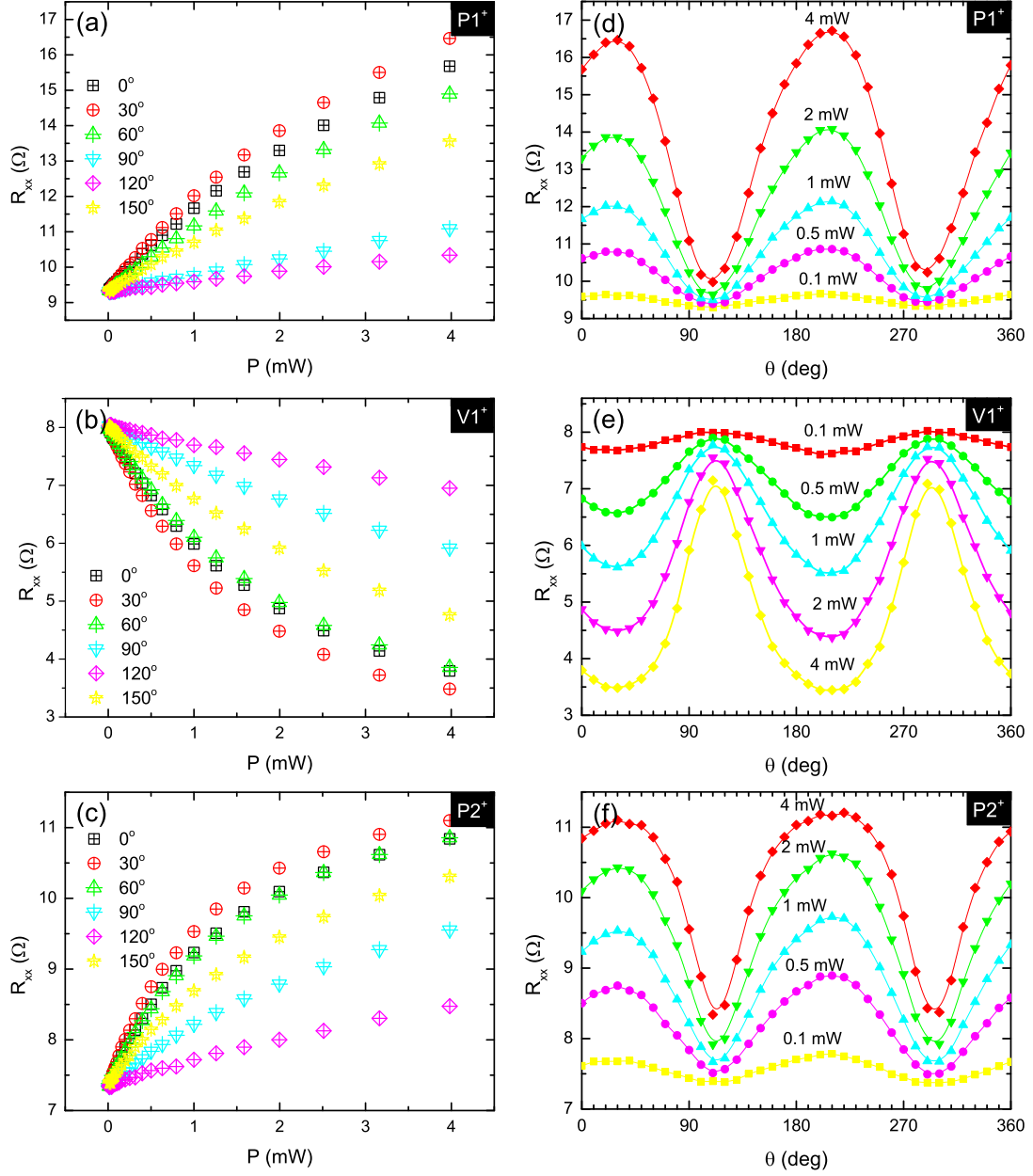
Figure 3.9. Panels (a)-(c) show the microwave power dependence at different polarization angles marked in Fig. 3.8 by vertical lines. Panels (d)-(f) show the microwave polarization dependence at different microwave powers marked in Fig. 3.8 by horizontal lines.

mobility 2DES in the regime of MRIMOs. (e) R_{xx} vs P curves at different polarization angles exhibit different non-linearity. (f) The difference in the non-linearity of the R_{xx} power dependence at different polarization angles is the factor that makes R_{xx} vs θ deviate from a cosine square function at high microwave powers.

The first two points can be compared with the prediction of the displacement model [44, 46, 48] and the radiation driven electron orbital model [50] regarding the power-dependence and polarization-dependence of the MRIMOs. The displacement model [44, 46, 48] suggests that microwave photo-excited electrons are scattered by impurities, and this gives rise to an additional current density due to radiation. Although ref. [48] disregarded the influence of the microwave radiation polarization, it did consider the role of the microwave power: for electron transitions between non-adjacent Landau levels, theory suggested "a linear dependence of σ_{ph} (photo-conductivity) and P in a wider range of microwave powers" [48] at the extrema of microwave radiation-induced oscillations. However, in the case of transitions between neighbouring Landau levels, theory indicated that the σ_{ph} vs. P dependence is non-linear at the extrema of microwave radiation-induced magneto-resistance oscillations with

$$|\sigma_{ph}| \propto P^{-1/2} \tag{3.3}$$

especially at high power. In Lei's expression of the displacement model [46], the magnitude of this photo-excited current density is a function of the polarization angle. However, we could not find a clear prediction regarding how, quantitatively, the microwave power at different polarization angles influences the photo-excited current density. The radiation driven electron orbital model [50] describes a periodic back- and forth- radiation driven motion of the electron orbits and the conductivity modulation resulting from the average coordinate change (scattering jump). This model shows both a non-linear power dependence and a linear polarization angle dependence, similar to experiment. On the other hand, the inelastic model [51] for magneto-oscillations in the photo-conductivity of the 2DES, which is governed by the microwave-induced change in the distribution function, suggests a linear dependence in the amplitude with the microwave power that is independent of the linear microwave polarization.

Regarding point (c), the point that the R_{xx} vs. P curves at different polarization angles θ are really just manifestations of the same curve can be understood as follows: In our experiment, the

transverse electric mode is excited by the MW antenna of Fig. 3.1(a) and the specimen is subject to the TE_{11} mode of the circular waveguide. The electric field along the device axis or the effective electric field E_e, see Fig. 1(a), is

$$E_e = E \cos \theta \tag{3.4}$$

where E is applied AC electric field. Since the measurements are reported as a function of the microwave power, which is the experimental variable, one might define an effective power,

$$P_e \propto E_e^2. \tag{3.5}$$

Then,

$$P_e = P \cos^2 \theta \tag{3.6}$$

gives the relation between the effective and applied microwave power and the polarization angle. The results, see Fig. 3.4, show that P/P_s normalizes microwave power with different polarization angles to the same effective power scale, making the R_{xx} vs P/P_s curves overlap each other (Fig. 3.5). Further, Fig. 3.6 shows that $1/P_s$ vs. θ can be fit $1/P_s(\theta) = A + C \cos^2(\theta - \theta_0)$. This confirms a possible role of a device parallel electric field. Fig. 3.6 also indicates that the phase shifts of this power scaling factor deviates at most by small angles from 0°, which suggests that the zero polarization angle mostly yields the maximum effective power in the present samples.

Regarding the microwave power dependence and linear polarization dependence of MRIMOs, previous studies [30, 34, 56, 64, 68] have also drawn the conclusion that at the magnetic fields corresponding to the extrema of MRIMOs, the R_{xx} varies non-linearly with P and the extremal R_{xx} follows $R_{xx}(\theta) = A \pm C cos^2(\theta - \theta_0)$ at low P. Regarding the polarization dependent distortion from cosine square function at high microwave power range, one must consider power and polarization angle together as point (d) suggested. Among the available theoretical models, few have considered both power dependence and polarization dependent at once. One model that considers them both is the radiation driven electron orbital model [50], which describes a periodic back-and-forth radiation-driven motion of the electron orbits and the conductivity modulation resulting from the average scattering jump. Simulations based on this model indicate a non-linear power dependence

of MRIMOs [56], i.e.,

$$A = A_0 P^\alpha \tag{3.7}$$

where A is the amplitude of, A_0 and $\alpha \approx 1/2$ are constants and P is microwave power. Moreover, the polarization dependence simulation [68] appears to suggest a distorted cosine square function. It seems plausible that if microwave power and polarization angle are considered together, this theory might model the power and polarization dependence of microwave-induced oscillatory magneto-resistance. The displacement model [44–46], which describes microwave photo-excited electrons scattered by impurities, and gives rise to an additional current density due to radiation, also considered the polarization dependence as sinusoidal [64]. However, this simulation did not include the power dependence. Also, the microwave intensities used in this simulation are quite different from the experimental intensities. Another displacement model simulation [48] has also studied the microwave power dependence of MRIMOs. They stated that photo-conductivity σ_{ph}, at extrema of MRIMOs, is a non-linear function of microwave power in the electron transition between adjacent Landau levels. This non-linearity is apparent especially at high microwave power range. However, this displacement model simulation indicated neither the polarization dependence nor its distortion due to high power. One might expect, however, to see the polarization dependent curve distortion at relative high microwave power in simulations utilizing the displacement model. Most other theoretical models have not predicted the polarization dependence of MRIMOs, not to mention the R_{xx} vs θ line shape distortion due to high microwave power.

3.5 Conclusion

In conclusion, microwave power dependence and linear polarization dependence studies of the radiation-induced oscillatory magneto-resistance in high quality GaAs/AlGaAs 2DES indicate a non-linear variation in the amplitude of the radiation-induced magneto-resistance oscillations with the microwave power at the oscillatory extrema along with a cosine squared dependence on the polarization angle. Furthermore, an empirically defined power scaling factor for normalizing the R_{xx} vs. P traces obtained at different linear microwave polarization angles also follows the cosine square function. This latter feature suggests a possible role for the device parallel component of electric field in influencing photo-excited electron transport. However, because the phase shifts θ_0

are different at different magnetic fields, there could also be other factors, other than the cosine component of electric field, that also play a role in the observed response. After further examining the evolution of the line shape of R_{xx} vs θ in MRIMOs with P using color contour plots of R_{xx} as a function of both microwave power P and linear polarization angle θ, the non-linearity of R_{xx} vs. P relation at different polarization angles is found to be the main factor that influences line shape distortion of the sinusoidal R_{xx} vs. θ relation.

Chapter 4

COMPARATIVE STUDY OF MRIMOS INDUCED BY CIRCULARLY- AND LINEARLY- POLARIZED PHOTO-EXCITATION

4.1 Introduction

The role of the polarization angle in experiments that utilize linearly polarized microwave photo-excitation has been a topic of interest in recent work [32, 34, 64, 68]. Associated experiments have shown, remarkably, that the amplitude of the radiation-induced magnetoresistance oscillations varies sinusoidally with the linear polarization angle, following a cosine-square function [34]. So far as circularly polarized microwave photo-excitation is concerned, there is only one experimental study [21] examining the magnetotransport response under circular polarization. This study focused on the microwave assisted cyclotron resonance and reported on the character of the radiation-induced magnetoresistance oscillations for left-hand and right-hand circularly polarized radiation. On the theoretical side, Lei and Liu [49, 69] examined radiation-induced magnetoresistance oscillations under a variety of polarization conditions, including linearly polarized microwaves with difference polarization directions, and circularly polarized microwaves with left handed and right handed orientations [49, 69]. They found that the amplitude of the magnetoresistance oscillations differs with the type of polarization of the radiation.

To complement this prior work, we have carried out a systematic comparative study of radiation-induced magnetoresistance oscillations using circularly polarized- and linearly polarized-microwaves, measured in the same sample, in a single cooldown, under nearly the same experimental conditions. The results show a striking sensitivity in the amplitude of the radiation-induced magnetoresistance oscillations under launcher rotation for linearly polarized microwaves, which is absent in the similar experiment carried out with circularly polarized microwaves. In addition, nearly similar response is observed in the cyclotron resonance active- and inactive- conditions for the circularly polarized radiation at the examined frequencies.
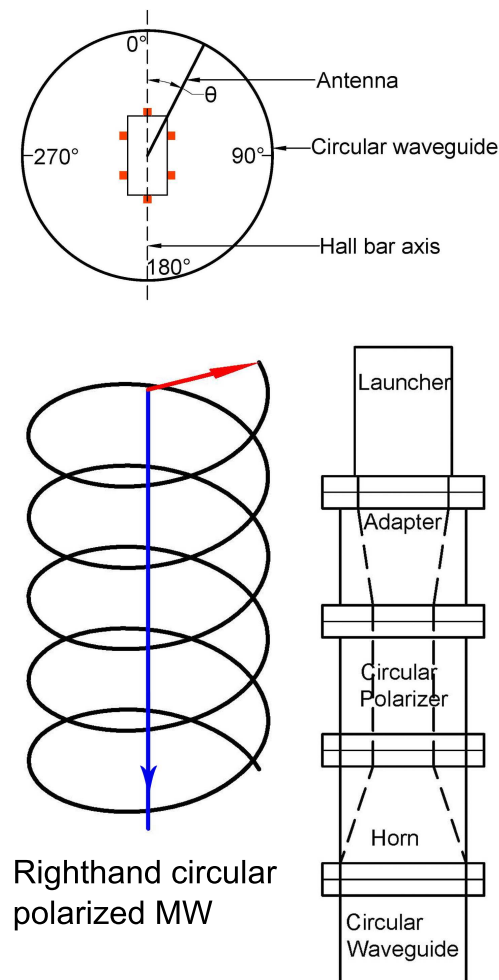
Figure 4.1. The experimental setup for producing- and conveying- circularly polarized microwaves. Top: The Hall bar sample is centered with respect to a circular waveguide. The electric-dipole antenna that generates linearly polarized microwave radiation can be rotated with respect to the Hall bar axis. Bottom-right: The scheme for converting launcher-generated linearly polarized microwaves into circularly polarized microwaves using a commercially available adapter, circular polarizer, and microwave horn. This adapter, polarizer, and horn assembly are inserted for the circular polarization measurements. Bottom-left: This figure indicates the electric field and the propogation direction of right-handed circularly polarized microwaves. The red arrow indicates the direction of the electric field and the blue arrow indicates the direction of transmission, which is parallel to the axis of the circular waveguide.

4.2 Linearly and circularly polarized microwave setup

The high mobility GaAs/AlGaAs heterojunction samples measured here were fabricated in the same way as stated in the second chapter. Basic low temperature, low noise, magneto-transport measurements here are the same as the previous chapter. For the linearly polarized microwaves, the microwave launcher was connected with the circular waveguide via a rectangular- to circular-waveguide adaptor. And for the circularly polarized microwaves, a commercially available circular polarizer with a microwave horn was inserted between adaptor and circular waveguide, see Fig. 4.1. The circular polarizer converts the linearly polarized microwaves generated by the launcher to right-hand circularly polarized microwaves over the frequency band between 43 GHz and 50 GHz.

In order to determine whether the microwave polarizers functioned as expected, a microwave power detector was installed at the nominal sample position, and the launcher angle was rotated by rotating the launcher assembly above the circular waveguide, see Fig. 4.1. Here, the launcher angle is defined as the angle between the antenna and a reference mark, which corresponds to $\theta = 0$, on the circular waveguide. After these preliminary detected-power-measurements, the power detector was replaced by the Hall bar sample, with the long axis of the Hall bar aligned along the $\theta = 0$ direction. Fig. 4.2(a) exhibits the detected power vs. the launcher angle for both linearly- and circularly- polarized 45.2 GHz microwave radiation, as measured by the microwave power detector. Here, the black trace shows the detected microwave power signal in the absence of microwaves. The blue curve shows the detected microwave power with linearly polarized microwaves. This microwave power signal exhibits a sinusoidal variation with the launcher angle and the highest detected power occurs at around $\theta = 0$, which indicates that launcher-antenna is parallel to the detector-antenna for maximum response. The red curve exhibits the detected microwave power vs. launcher angle for circularly polarized microwaves. The red trace shows that the detected power for circularly polarized microwaves is insensitive to the launcher angle and the detected power in this instance is 2/3 of the average detected power for linearly polarized microwaves. At $\theta = 0$, the detected power signal was also measured as a function of the microwave source-power, these results are shown in Fig. 4.2(b). From Fig. 4.2(b), it is clear that at the bottom end of the circular waveguide sample holder, the detected microwave power changes linearly with the microwave source power, for both linearly polarized- or circularly polarized- microwave radiation.
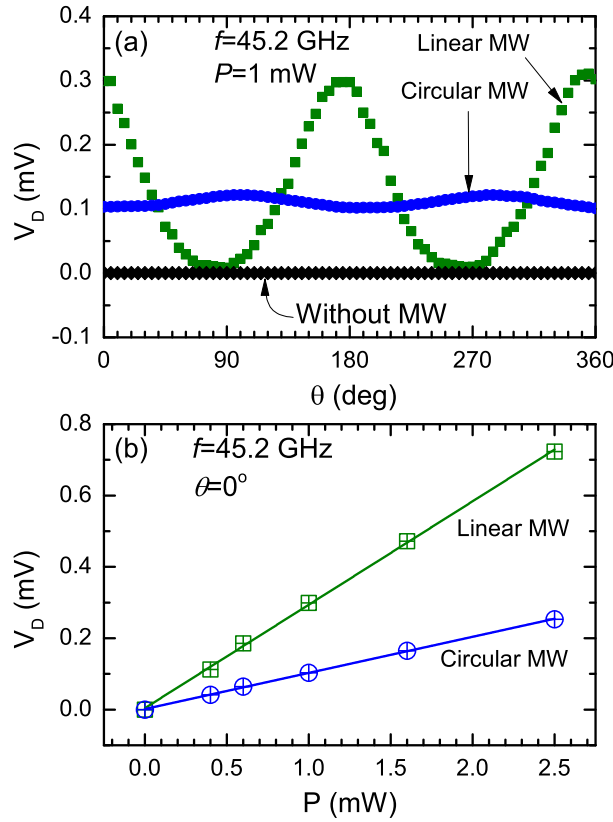
Figure 4.2. (a) The observed microwave power detector response as a function of the launcher-antenna-angle when a microwave power detector is placed at the bottom of the sample holder, at the nominal position of the sample, for circularly- and linearly- polarized microwave radiation. Here, the measurements were carried out with 45.2 GHz microwave radiation at a power level P = 1 mW. The results for linearly polarized microwaves are represented with green symbols while the results for circularly polarized microwaves are represented with blue symbols. The black trace shows the power detector response in the absence of microwave radiation. (b) Microwave power detector response as a function of source microwave power for linearly (green) and circularly (blue) polarized microwave at a 0° polarization angle.

4.3   Results
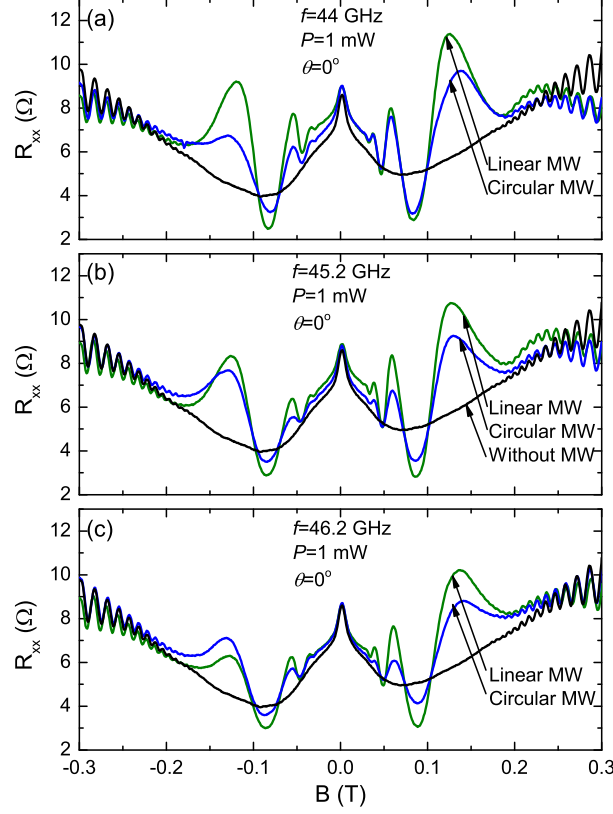
Figure 4.3.   (a) Magnetoresistance measurements under microwave photoexcitation for a GaAs/AlGaAs 2DES specimen at (a) f=44 GHz with P= 1 mW, (b) f=45.2 GHz with P= 1 mW and (c) f= 46.2 GHz with P= 1 mW. Green curves represent measurements with linearly polarized microwaves, blue curves represent measurements with circularly polarized microwaves, and the black curve represents measurements without microwave excitation.

Figure 4.3 compares the observed microwave induced magnetoresistance oscillations under linearly- and circularly-polarized microwave excitation at $f = 44$, 45.2, and 46.2 GHz. Here, similar B^{-1}-periodic and 1/4-cycle shifted magnetoresistance oscillations are observed for both linearly- and circularly- polarized radiation, as the peaks and valleys shift together in the same way on B axis as radiation-frequency changes in both cases. As well, there are some perceptible differences in the amplitude of the magnetoresistive response for the two two types of polarizations. At every frequency, the amplitude of the microwave induced oscillatory magnetoresistance for circularly polarized microwaves is generally smaller than the amplitude of the oscillatory magnetoresistance induced by linearly polarized microwaves. An exception here is the first peak observable at $B = -0.125$ Tesla

at 46.2 GHz, see Fig. 4.3(c). Although the height of this resistance peak is higher for circularly polarized radiation than it is for linearly polarized radiation, the total amplitude of the corresponding oscillation is nearly the same for the two polarizations. Here, it should be noted that although the source power is the same, i.e., $P = 1$ mW, for the measurements with linearly and circularly polarized radiation, the power at the sample will not be the same since additional hardware, in the form of the circular polarizer and horn, used for the circular polarization measurements, introduces insertion loss and associated power attenuation.

Figure 4.4. Magneto-resistance traces at different microwave power levels for (a) linearly polarized and (b) circularly polarized microwave radiation. (c) The diagonal resistance is shown as a function of the microwave power for linearly (blue) and circularly (red) polarized microwaves. These data were extracted from (a) and (b) at the magnetic field corresponding to P2+.
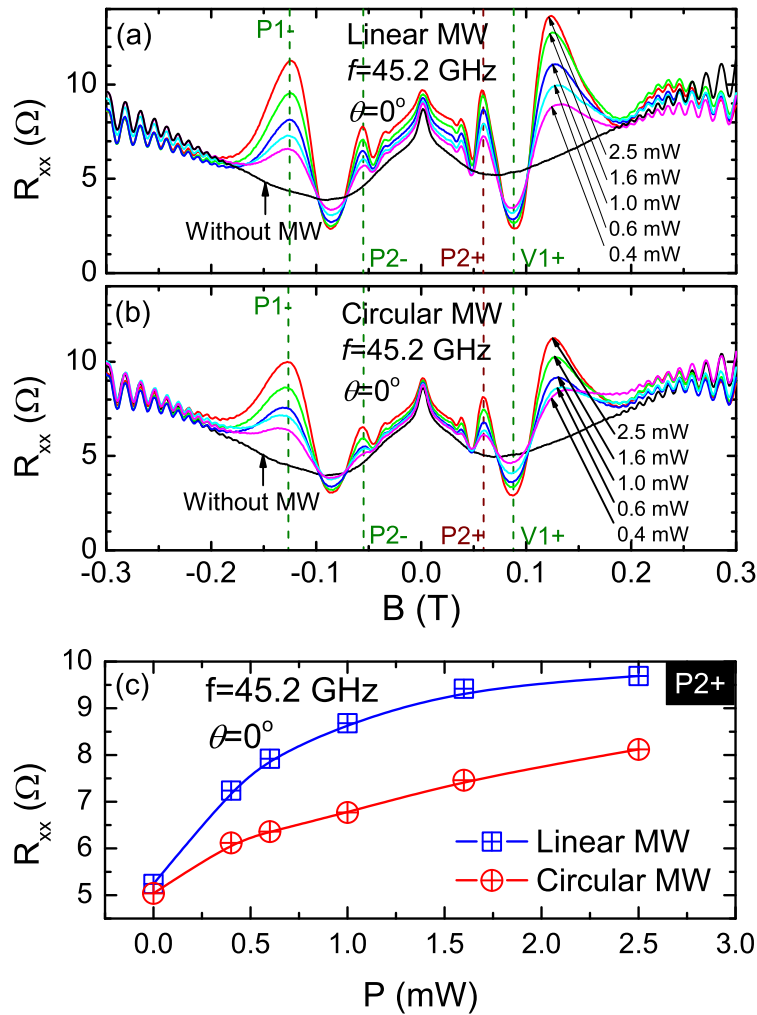
Figures 4.4 (a) and (b) show R_{xx} vs. B at a number of power levels, P, for both linearly and circularly polarized microwaves at 45.2 GHz. Here, as the microwave power increases, the oscillatory amplitude increases for both linearly- and circularly- polarized radiation. The power dependence of the peak resistance labeled $P2+$, shown in Fig. 4.4(c), indicates a non-linear increase in the peak resistance with power in the two cases. Note that, in Fig. 4.4(c), the R_{xx} vs P traces for the linearly- and circularly- polarized radiation start similarly but then diverge at higher source power. This feature indicates that less excitation is being coupled into the physical mechanism responsible for the radiation-induced magnetoresistance oscillations in the case of circularly polarized radiation.
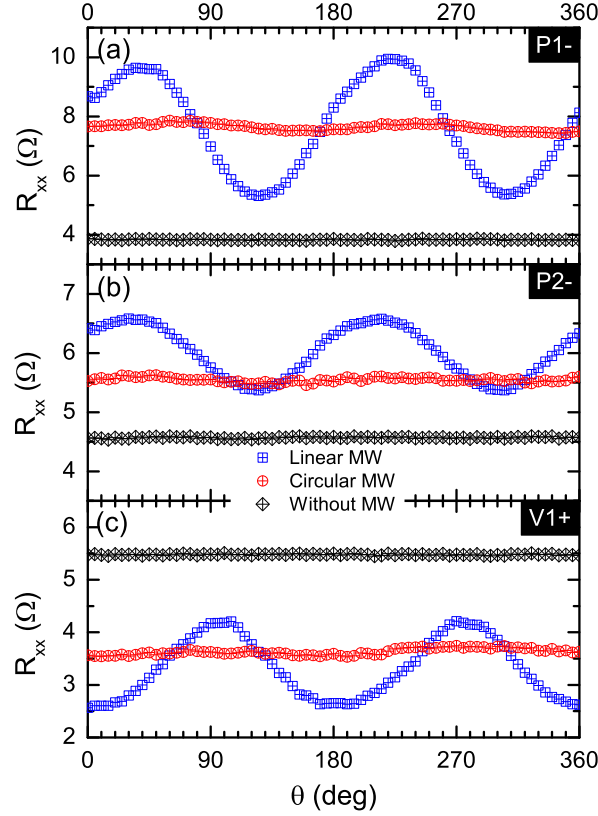
Figure 4.5. Panels (a)-(c) show the diagonal resistance as a function of the antenna angle for $f=$ 45.2 GHz radiation with source power $P = 1$ mW for both linearly polarized (blue symbols) and circularly polarized (red symbols) microwaves at (a) P1-, (b) P2- and (c) V1+. The responses in the absence of microwaves, i.e., dark, are shown in black. Here, the magnetic fields corresponding to P1-, P2- and V1+ are marked Fig. 4.4 (a) and (b).

Figures 4.5(a) to (c) show the launcher-angle-dependence of the radiation-induced magnetore-sistance oscillations for the linearly- and circularly-polarized radiations at the magnetic fields labeled as P1-, P2- and V1+, indicated as dashed lines in Fig. 4.4(a) and (b). Fig. 4.5(a)-(c) shows that

for linearly polarized radiation, the magnetoresistive response at the oscillatory peaks and valleys varies sinusoidally with the launcher angle as reported previously [34]. In sharp contrast, for circularly polarized radiation, the magnetoresistive response at the peaks and valleys hardly shows any launcher angle dependence; there appears to be a nearly constant response as a function of launcher angle. Finally, at a given peak or valley of the radiation-induced oscillatory magnetoresistance, the data for the circular polarization lie between the peak and valley of the oscillatory data for the linearly polarized radiation.

4.4   Discussion

This study has compared the magneto-resistive response of the high mobility GaAs/AlGaAs 2D electron system under linearly- and circularly- polarized microwave photo-excitation in the frequency band spanning $43 \leq f \leq 50$ GHz. The results show that (a) peaks and valleys in the radiation-induced oscillatory magneto-resistance shift to higher magnetic field with an increase in the microwave frequency for circularly polarized radiation, similar to the response for linearly polarized radiation. (b) The amplitude of the radiation-induced oscillatory magneto-resistance increases non-linearly with the microwave power for circularly polarized radiation, similar to the observed response for linearly polarized microwaves. (c) Upon rotating the microwave launcher, the amplitude of the radiation-induced magneto-resistance oscillations hardly changes with the launcher angle for circularly polarized radiation. Indeed, nearly the same oscillatory magneto-resistive response is observed at all launch angles for circularly polarized radiation. This feature is quite unlike the strong sinusoidal variation in the response with the launch angle observed for linearly polarized radiation.

Among existing theoretical models, the displacement model has examined in detail the effect of different types of microwave polarization. For example, Lei and Liu have considered photo-excitation with an ac electric field that follows

$$E = E_s \sin(\omega t) + E_c \cos(\omega t) \tag{4.1}$$

which can serve to represent both circularly- and linearly- polarized microwaves. The model simulation from this theory for linearly polarized radiation [64] indicates a sinusoidal magneto-resistance

change vs. the polarization angle, qualitatively similar to the results observed in experiment, see Fig. 4.5 (d) to (f). The model simulation for circularly polarized radiation [49, 69] produces magneto-resistance oscillations vs. the magnetic field that are qualitatively similar to that observed for linearly polarized radiation, as shown here. In addition, however, the model indicates a difference in the amplitude of the magneto-resistive response in the vicinity of cyclotron resonance for circular polarized radiation corresponding to the cyclotron-resonance active and inactive conditions, and also a difference in response for circularly- and linearly-polarized radiation. In the present experiment, the right hand circularly polarized microwaves correspond to the cyclotron resonance inactive condition at positive magnetic field because the polarization direction is against the cyclic motion of electrons. On the other hand, at negative magnetic field, the right hand polarized microwaves correspond to the cyclotron resonance active condition. Thus, the theory suggests a possible greater response in the vicinity of cyclotron resonance at negative magnetic fields in our experiments. Our results show, however, that the magneto-resistive oscillatory amplitudes for circularly polarized radiation are comparable for positive and negative magnetic fields. This feature seems to indicate that cyclotron resonance activity or inactivity of circularly polarized microwaves produces a small or no response in the vicinity of cyclotron resonance, at least at the microwave frequencies examined in this experiment.

The microwave driven electron orbital model [68] has considered microwave electric fields that satisfy

$$\overrightarrow{E}(t) = (E_{0x} \overrightarrow{i} + E_{0y} \overrightarrow{j}) \cos(\omega t) \tag{4.2}$$

which correspond to linearly polarized microwave radiation with a polarization angle α given by the relation

$$\tan \alpha = \frac{E_{0y}}{E_{0x}}. \tag{4.3}$$

This model successfully predicted the linear polarization angle dependence of MRIMOs. As well, it has been successful in describing the power dependence [56] with linearly polarized microwave radiation. It would be interesting for this model to examine in depth the model expectations for circularly polarized microwave radiation.

To our knowledge, the inelastic model has not examined the linear- vis-a-vis circular- polarization issue at great depth since the theory indicates an absence of polarization sensitivity in (and a linear power dependence of) the radiation-induced magneto-resistance oscillations.

4.5 Conclusion

A comparative study of the radiation-induced magneto-resistance oscillations under linearly- and circularly- polarized microwave excitation indicates similar basic features in the observed oscillatory magneto-resistive response such as periodicity in B^{-1}, a 1/4-cycle phase shift, and non-linear increase in the amplitude of the oscillations with the microwave power for the two types of radiations. There is, however, a profound difference in the response observed upon rotating the microwave launcher for the linearly- and circularly- polarized radiations. For the linearly polarized radiation, the magneto-resistive response is a strong sinusoidal function of the launcher rotation (or linear polarization) angle, θ. On the other hand, for circularly polarized radiation, the oscillatory magneto-resistive response is hardly sensitive to θ. Finally, for circular polarized radiation, the magneto-resistive response for the cyclotron resonance active and inactive conditions is approximately the same over the entire field range. There could be a small difference in the immediate vicinity of cyclotron resonance. This feature is, at present, the topic of a more detailed investigation.

Chapter 5

SUMMARY

In summary, this dissertation addressed mainly three experimental questions regard MRIMOs: a)microwave reflection from 2DES, b) the combined effect of microwave power and microwave polarization on the transport of 2DES and, c) the change of MRIMOs under different microwave polarizations.

In the microwave reflection measurement, we used different methods (carbon sensor and microwave power meter) to demonstrate a strong correlation between the magneto-resistive and the concurrent microwave reflection from the microwave photo-excited GaAs/AlGaAs 2DES. These correlations are followed as a function of the microwave power, the microwave frequency, and the applied current. Notably, the character of the reflection signal remains unchanged even when the current is switched off in the GaAs/AlGaAs Hall bar specimen. The results suggest a perceptible microwave-induced change in the electronic properties of the 2DES, even in the absence of an applied current. In addition, the oscillatory remotely sensed signal is shown to exhibit a power law type variation in its amplitude, similar to the radiation-induced magneto-resistance oscillations. Related works have been published [39, 40].

In the combined study of microwave power and polarization on the transport of 2DES, we report a combined microwave polarization-dependence-and power- dependence study of the MRIMOs in high mobility GaAs/AlGaAs heterostructure devices at liquid helium temperatures. The diagonal resistance was measured with the magnetic field fixed at the extrema of the radiation-induced magnetoresistance oscillations, as the microwave power was varied at a number of microwave polarization angles. The results indicate a non-linear relation between the oscillatory peak- or valley-magnetoresistance and the microwave power, as well as a cosine square relation between the oscillatory peak- or valley- magnetoresistance and the microwave polarization angle. The main features are briefly compared with the predictions of existing models. In the later part of this study we examine the role of the microwave power in the linear polarization angle dependence of the microwave radiation induced magnetoresistance oscillations observed in the high mobility GaAs/AlGaAs two

dimensional electron system. Diagonal resistance R_{xx} was measured at fixed magnetic fields corresponding to the photo-excited oscillatory extrema of R_{xx} as a function of both the microwave power, P, and the linear polarization angle, θ. Color contour plots of such measurements demonstrate the evolution of the R_{xx} versus θ line shape with increasing microwave power. We report that the non-linear power dependence of the amplitude of the radiation-induced magnetoresistance oscillations distorts the cosine-square relation between R_{xx} and θ at high power. Related works have been published [41, 42]

In the microwave polarization study of MRIMOs, we comparatively studied the radiation-induced magnetoresistance oscillations in the high mobility GaAs/AlGaAs heterostructure 2DES under linearly- and circularly- polarized microwave excitation. The results indicate a profound difference in the response observed upon rotating the microwave launcher for the two cases, although circularly polarized microwave radiation induced magnetoresistance oscillations observed at low magnetic fields are similar to the oscillations observed with linearly polarized radiation. For the linearly polarized radiation, the magnetoresistive response is a strong sinusoidal function of the launcher rotation (or linear polarization) angle, θ. For circularly polarized radiation, the oscillatory magnetoresistive response is hardly sensitive to θ. The results also suggest that for circular polarized radiation, the magnetoresistive response is approximately the same for the cyclotron resonance active and inactive conditions over the entire magnetic field range at the examined frequencies.

These research projects about MRIMOs provide the necessary information to explore the real physical explanations of such a phenomenon. As well, these studies have included different microwave power, different microwave polarizations and even the microwave reflection behaviour from MRIMOs in high mobility 2DES. The results of this dissertation will contribute to the application of 2DES for microwave or terahertz wave detection and other possible applications.

The journal publications and conference presentations related to my Ph.D. works are listed together at the end of the reference [71–93].

REFERENCES

[1] K. von Klitzing, G. Dorda, and M. Petter,Phys. Rev. Lett. **45**, 494 (1980).

[2] D. C. Tsui, H. L. Stormer, and A. C. Gossard, Phys. Rev. Lett. **48**, 1559 (1982).

[3] R. B. Laughlin, Physs. Rev. Lett. **50**, 1395 (1983).

[4] R. G. Mani, J. H. Smet, K. von Klitzing, V. Narayanamurti, W. B. Johnson, and V. Umansky, Nature **420**, 646 (2002).

[5] K. S. Novoselov, A. K. Geim, S. V. Morozov, D. Jiang, M. I. Katsnelson, I. V. Grigorieva, S. V. Dubonos, and A. A. Firsov, Nature **438**, 197 (2005).

[6] A. Y. Cho, Materials Research Society (MRS) Bulletin **20**, 21 (1995).

[7] "Klaus von Klitzing -Nobel Lecture: The Quantized Hall Effect". Nobelprize.org. Nobel Media AB 2014. Web. 23 Apr 2015.
$http : //www.nobelprize.org/nobel_prizes/physics/laureates/1985/klitzing − lecture.html$

[8] "HALL EFFECT-Explanation of the Quantum Hall Effect"
$http : //www.referatele.com/referate/fizica/online4/HALL−EFFECT−−−Explanation$
$− of − the − Quantum − Hall − Effect − referatele − com.php$

[9] M. A. Zudov, R. R. Du, L. N. Pfeiffer, and K. W. West, Phys. Rev. Lett. **90**, 046807 (2003).

[10] R. G. Mani, J. H. Smet, K. von Klitzing, V. Narayanamurti, W. B. Johnson, and V. Umansky, Phys. Rev. Lett. **92**, 146801 (2004).

[11] R. G. Mani, J. H. Smet, K. von Klitzing, V. Narayanamurti, W. B. Johnson, and V. Umansky, Phys. Rev. B **69**, 193304 (2004).

[12] R. G. Mani, V. Narayanamurti, K. von Klitzing, J. H. Smet, W. B. Johnson, V. and Umansky, Phys. Rev. B **69**, 161306 (2004).

[13] R. G. Mani, Physica E **22**, 1 (2004); Physica E. **25**, 189 (2004).

[14] R. G. Mani, V. Narayanamurti, K. von Klitzing, J. H. Smet, W. B. Johnson, and V. Umansky, Phys. Rev. B **70**, 155310 (2004); Phys. Rev. B **69**, 161306 (2004).

[15] R. G. Mani, Appl. Phys. Lett. **85**, 4962 (2004).

[16] R. G. Mani, Inte. J of Mode. Phys. B **18**, 3473 (2004).

[17] A. E. Kovalev, S. A. Zvyagin, C. R. Bowers, J. L. Reno, and J. A. Simmons, Solid State Commun. **130**, 379 (2004).

[18] R. G. Mani, Phys. Rev. B **72**, 075327 (2005); Appl. Phys. Lett. **91**, 132103 (2007); Physica E **40**, 1178 (2008).

[19] S. A. Studenikin, M. Potemski, A. Sachrajda, M. Hilke, L. N. Pfeiffer, and K. W. West, Phys. Rev. B **71**, 245313 (2005).

[20] B. Simovic, C. Ellenberger, K. Ensslin, H. P. Tranitz, and W. Wegscheider, Phys. Rev. B **71**, 233303 (2005).

[21] J. H. Smet, B. Gorshunov, C. Jiang, L. Pfeiffer, K. West, V. Umansky, M. Dressel, R. Meisels, F. Kuchar, and K. von Klitzing, Phys. Rev. Lett. **95**, 116804 (2005).

[22] R. G. Mani, Appl. Phys. Lett. **91**, 132103 (2007).

[23] A. Wirthmann, B. D. McCombe, D. Heitmann, S. Holland, K. Friedland, and C. M. Hu, Phys. Rev. B **76**, 195315 (2007).

[24] S. A. Studenikin *et al.*, Phys. Rev. B **76**, 165321 (2007).

[25] R. G. Mani, Appl. Phys. Lett. **92**, 102107 (2008).

[26] S. Wiedmann, G. M. Gusev, O. E. Raichev, T. E. Lamas, A. K. Bakarov, and J. C. Portal, Phys. Rev. B **78**, 121301 (2008).

[27] R. G. Mani, Appl. Phys. Lett. 92, 102107 (2008).

[28] D. Konstantinov and K. Kono, Phys. Rev. Lett. **103**, 266808 (2009).

[29] R. G. Mani, W. B. Johnson, V. Umansky, V. Narayanamurti, and K. Ploog, Phys. Rev. B **79**, 205320 (2009).

[30] R. G. Mani, C. Gerl, S. Schmult, W. Wegscheider, and V. Umansky, Phys. Rev. B **81**, 125320 (2010).

[31] O. M. Fedorych, M. Potemski, S. A. Studenikin, J. A. Gupta, Z. R. Wasilewski, and I. A. Dmitriev, Phys. Rev. B **81**, 201302 (2010).

[32] R. G. Mani, A. N. Ramanayaka, and W. Wegscheider, Phys. Rev. B **84**, 085308 (2011).

[33] A. N. Ramanayaka, R. G. Mani, and W. Wegscheider, Phys. Rev. B **83**, 165303 (2011).

[34] A. N. Ramanayaka, R. G. Mani, J. Iñarrea, and W. Wegscheider, Phys. Rev. B **85**, 205315 (2012).

[35] R. G. Mani, J. Hankinson, C. Berger, and W. A. de Heer, Nat. Commun. **3**, 996 (2012).

[36] R. G. Mani, A. Ramanayaka, T. Ye *et. al.*, Phys. Rev. B **87**, 245308 (2013).

[37] R. G. Mani, A. Kriisa, and W. Wegscheider, Sci. Rep. **3**, 2747 (2013).

[38] R. G. Mani and A. Kriisa, Sci. Rep. **3**, 3478 (2013).

[39] T. Ye, R. G. Mani, and W. Wegscheider, Appl. Phys. Lett. **102**, 242113 (2013).

[40] T. Ye, R. G. Mani, and W. Wegscheider, Appl. Phys. Lett. **103**, 192106 (2013).

[41] T. Ye, H.C. Liu, W. Wegscheider, and R. G. Mani, Phys. Rev. B **89**, 155307 (2014).

[42] T. Ye, W. Wegscheider, and R. G. Mani, Appl. Phys. Lett. **105**, 191609 (2014).

[43] H.C. Liu, T. Ye, W. Wegscheider, and R. G. Mani, J. Appl. Phys. **117**, 064306 (2015).

[44] A. C. Durst, S. Sachdev, N. Read, and S. M. Girvin, Phys. Rev. Lett. **91**, 086803 (2003).

[45] V. Ryzhii and R. Suris, J. Phys. Condens. Matter **15**, 6855 (2003).

[46] X. L. Lei and S. Y. Liu, Phys. Rev. Lett. **91**, 226805 (2003).

[47] A. V. Andreev, I. L. Aleiner, and A. J. Millis, Phys. Rev. Lett. **91**, 056803 (2003).

[48] V. Ryzhii, Phys. Rev. B **68**, 193402 (2003).

[49] X. L. Lei and S. Y. Liu, Phys. Rev. B **72**, 075345 (2005).

[50] J. Iñarrea and G. Platero, Phys. Rev. Lett. **94**, 016806 (2005); Phys. Rev. B **76**, 073311 (2007).

[51] I. A. Dmitriev, M. G. Vavilov, I. L. Aleiner, A. D. Mirlin, and D. G. Polyakov, Phys. Rev. B **71**, 115316 (2005).

[52] A. A. Koulakov and M. E. Raikh, Phys. Rev. B **68**, 115324 (2003).

[53] A. D. Chepelianskii, A. S. Pikovsky, and D. L. Shepelyansky, Eur. Phys. J. B **60**, 225 (2007).

[54] I. G. Finkler and B. I. Halperin, Phys. Rev. B **79**, 085315 (2009).

[55] A. D. Chepelianskii and D. L. Shepelyansky, Phys. Rev. B **80**, 241308 (2009).

[56] J. Iñarrea, R. G. Mani, and W. Wegscheider, Phys. Rev. B **82**, 205321 (2010).

[57] J. Inarrea and G. Platero, Nanotechnology **21**, 315401 (2010).

[58] D. Hagenmüller, S. De Liberato, and C. Ciuti, Phys. Rev. B **81**, 235303 (2010).

[59] X. L. Lei, Mat. Sci. Eng. R **70**, 126 (2010).

[60] S. A. Mikhailov, Phys. Rev. B **83**, 155303 (2011).

[61] Z. Gu, H. A. Fertig, D. P. Arovas, and A. Auerbach, Phys. Rev. Lett. **107**, 216601 (2011).

[62] N. H. Lindner, G. Refael, and V. Galitski, Nat. Phys. **7**, 490 (2011).

[63] X. L. Lei and S. Y. Liu, Phys. Rev. B **84**, 035321 (2011); Phys. Rev. B **86**, 205303 (2012).

[64] X. L. Lei and S. Y. Liu, Phys. Rev. B **86**, 205303 (2012).

[65] J. Iñarrea, Appl. Phys. Lett. **100**, 242103 (2012).

[66] A. Kunold and M. Torres, Physica B **425**, 78 (2013).

[67] O. V. Zhirov, A. D. Chepelianskii, and D. L. Shepelyansky, Phys. Rev. B **88**, 035410 (2013).

[68] J. Iñarrea,J. Appl. Phys. **113**, 183717 (2013).

[69] X. L. Lei and S. Y. Liu,Infrared, Millimeter, and Terahertz Waves (IRMMW-THz), 2013 38th International Conference pp.1,2, 1-6 Sept. 2013.

[70] J. Iñarrea, Nano. Res. Lett. **8**, 259 (2013).

[71] H. C. Liu, T. Ye, W. Wegscheider, and R. G. Mani, J. Appl. Phys. **117**, 064306 (2015).

[72] T. Ye, W. Wegscheider, and R. G. Mani, Appl. Phys. Lett. **105**, 191609 (2014).

[73] A. N. Ramanayaka, T. Ye, H-C. Liu, W. Wegscheider, and R. G. Mani, Physica B **453**, 43-48 (2014).

[74] T. Ye, H. C. Liu, W. Wegscheider, and R. G. Mani, Phys. Rev. B **89**,155307 (2014).

[75] T. Ye, R. G. Mani, and W. Wegscheider, MRS Proc. **1635**, mrsf13-1635-t09-05 (2014).

[76] T. Ye, R. G. Mani, and W. Wegscheider, AIP Conf. Proc. **1566**, 281 (2013).

[77] T. Ye, R. G. Mani, and W. Wescheider, Appl. Phys. Lett. **103**, 192106 (2013).

[78] T. Ye, R. G. Mani, and W. Wescheider, Appl. Phys. Lett. **102**, 242113 (2013).

[79] R. G. Mani, A. N. Ramanayaka, T. Ye, M. S. Heimbeck, H. O. Everitt, and W. Wegscheider, Phys. Rev. B **87**,245308 (2013).

[80] T. Ye, R. G. Mani, and W. Wegscheider, American Physical Society March meeting 2015, San Antonio, TX, March 3, 2015.

[81] T. Ye, H. C. Liu, R. G. Mani, and W. Wegscheider, 32nd International Conference on the Physics of Semiconductors (ICPS 2014), Austin, TX, August 12, 2014.

[82] T. Ye, H. C. Liu, R. G. Mani, and W. Wegscheider, The 21st International Conference on "High Magnetic Fields in Semiconductor Physics" (HMF-21), Panama City Beach, FL, August 6, 2014.

[83] T. Ye, R. G. Mani, and W. Wegscheider, American Physical Society March meeting 2014, Denver, CO, March 3, 2014.

[84] T. Ye, R. G. Mani, and W. Wegscheider, 2013 MRS Fall meeting, Boston, MA, December 4, 2013.

[85] T. Ye, R. G. Mani, and W. Wegscheider, XXII International Materials Research Congress 2013, Cancun, Mexico, August 14, 2013.

[86] T. Ye, R. G. Mani, and W. Wegscheider, 20th International Conference on Electronic Properties of Two-Dimensional Systems, Wroclaw, Poland, July 1, 2013.

[87] T. Ye, R. G. Mani, and W. Wegscheider, American Physical Society March meeting 2013, Baltimore, MD, March 18, 2013.

[88] T. Ye, R. G. Mani, and W. Wegscheider, 31st International Conference on The Physics of Semiconductors, Zurich, Switzerland, August 2, 2012.

[89] T. Ye, A. Ramanayaka, R. G. Mani and W. Wegscheider, The 20th International Conference on "High Magnetic Fields in Semiconductor Physics,Chamonix Mont-Blanc, France, July 26, 2012.

[90] T. Ye, R. G. Mani, and W. Wegscheider, 2012 International Workshop on Non-equilibrium Phenomena in Complex Quantum Systems in Japan, Okinawa Japan, April 25, 2012.

[91] T. Ye, A. Ramanayaka, R. G. Mani, and W. Wegscheider, American Physical Society March meeting 2012, Boston MA, March 1, 2012.

[92] T. Ye, G. Chand, A. Ramanayaka, R. G. Mani, and W. Wegscheider, 19th International Conference on Electronic Properties of Two-Dimensional Systems, Tallahassee FL, July 25, 2011.

[93] T. Ye, G. Chand, A. Ramanayaka, R. G. Mani, and W. Wegscheider, American Physical Society March meeting 2011, Dallas TX, March 24, 2011.